From Impact to Control: Inertially Amplified Friction Bearings

Sudip Chowdhury[1], Arnab Banerjee[2], and Sondipon Adhikari[3]

[1]Research Associate, PhD, James Watt School of Engineering, The University of Glasgow, Glasgow, Scotland, United Kingdom, Email Id: Sudip.Chowdhury@glasgow.ac.uk

[2]Assistant Professor, PhD, Civil Engineering Department, Indian Institute of Technology Delhi, India, Email Id: abanerjee@iitd.ac.in

[3]Professor of Engineering Mechanics, PhD, James Watt School of Engineering, The University of Glasgow, Glasgow, Scotland, United Kingdom, Email Id: Sondipon.Adhikari@glasgow.ac.uk

ABSTRACT

The conventional friction bearings have limitations in controlling the structures' vibration. To overcome their limitations and upgrade their seismic performances, the inertial amplifiers and inerters are applied to the core material of the conventional friction bearings. Accordingly, this paper introduces two kinds of upgraded friction bearings: inertial amplifier friction bearings and inerter-based friction bearings. These upgraded friction bearings are installed at the base of the single and multi-storey buildings with an adjacent retaining wall. The impact between the building and the retaining wall is considered. Following Newton's second law, the governing equations of motion for the isolated structures, including the impact, are derived. The impact is formulated by the "signum" function to derive analytical optimal closed-form solutions for the design parameters of these upgraded base isolators. H_2 and H_∞ optimisation methods are applied to derive the exact closed-form expression for the optimal design parameters. To employ the H_2 optimisation method, the statistical linearisation method is applied to linearise each nonlinear element of the governing equations of motion. Parametric studies show that optimum frequency and damping ratios decrease with increasing isolator mass ratio, increase with increasing inertial

angle, and decrease with increasing isolator mass ratio. Transfer function development is the first step in obtaining dynamic reactions of isolated structures. Furthermore, Newmark-beta method is employed to validate the results of the frequency domain analysis and obtained dynamic response histories for the isolated single-degree-of-freedom systems. According to the results, the dynamic response reduction capacities of the inerter-based friction bearing and inertial amplifier friction bearing are significantly 97.16 % and 96.62 % superior to the conventional base isolators. All results are mathematically derived and accurate; hence, applicable to practical implementations.

AUTHOR KEYWORDS

Upgraded friction bearings, Inertial amplifier friction bearings, Inerter-based friction bearings, "Signum" function, H_2 and H_∞ optimisation techniques, Dynamic response reduction capacities.

INTRODUCTION

A structural engineering method called base isolation (Kelly 1986), often referred to as seismic base isolation or base isolators, shields infrastructure and buildings from the destructive power of earthquakes (Jangid 2021). In order for a building or other structure to move independently of the ground motion during an earthquake, it must be supported by flexible bearings or isolators. Base isolation serves the main function of minimising structural damage and improving occupant safety by reducing the transfer of seismic forces and vibrations from the ground to the superstructure (Sharma and Jangid 2010). Base isolators might be friction pendulum bearings (Cardone et al. 2015), sliding bearings (Shrimali and Jangid 2002), and elastomeric bearings, among other types. These devices provide flexibility and dampening and are positioned between the superstructure and the foundation (Rahgozar et al. 2023). The ground shifts both vertically and horizontally during an earthquake. The superstructure may move independently of these ground movements thanks to base isolators, which lessens the chance that seismic forces and vibrations will enter the building. Base isolators lessen the amount of energy sent to the structure by dissipating energy via the deformation of its materials or sliding mechanisms (Liu et al. 2023). This dissipation of energy aids in shielding the structure from harm. Base isolation lowers the chance of major structural damage or building

collapse during an earthquake, which greatly increases occupant safety. Additionally, it enables a more predictable and regulated reaction to earthquake occurrences. Critical infrastructure, including emergency response centres, hospitals, and historic structures, often uses base isolation. It may also be used on a wide variety of other constructions, including industrial facilities, bridges, and residential buildings. When designing a base-isolated structure, the mass and stiffness of the building, the kind of isolators to be utilised, and the seismic hazard unique to the location must all be carefully taken into account (Zhao et al. 2021). The isolator's ability to efficiently absorb seismic energy and stop the superstructure from shifting too much must be guaranteed by the design. Resilient friction bearing isolators, often referred to as isolator mounts or just isolators, are mechanical parts that lessen shock and vibration transfer between a piece of machinery or equipment and the structure that supports it. These isolators are often used in a variety of industrial applications to shield delicate equipment, machinery, and buildings from the harmful effects of vibrations, such as those produced by spinning engines, machinery, or outside pressures (Mostaghel and Khodaverdian 1987). Rubber or neoprene, two elastomeric materials, are often used to make the robust aspect of the conventional base isolators. This part isolates vibrations and shocks by being flexible and having dampening qualities. The outside structure that secures the resilient part in place is the isolator's housing, which is usually composed of metal (Luo et al. 2023). To further reduce and manage vibrations, resilient friction bearing isolators (Chowdhury et al. 2023a) may include friction pads or shear components within the housing. In order to enable attachment to both the equipment and the supporting structure, isolators often have mounting holes or brackets. The weight of the equipment and the necessary degree of isolation must be taken into consideration when choosing an isolator since each one is designed to sustain a certain load capacity or weight (Ou et al. 2021).

The design parameters must be optimised for these isolators to provide a strong dynamic response reduction capacity. Among the popular analytical optimisation techniques is the H_2 optimisation approach (Chowdhury et al. 2023c). This approach allows for the derivation of the optimal design parameters in terms of closed-form equations. This technique may be used

for isolated structures that are randomly energised. Increasing the static mass of isolators is another way to get strong vibration reduction performance since this will overly enhance the base layer's flexibility during seismic events (Sun et al. 2019). H_∞ optimisation method is one of the prominent analytical optimisation methods to derive the optimal design parameters for the isolators (Chowdhury et al. 2024). Initially, the harmonic excitation needs to be employed as loading function to the isolator. Furthermore, the base isolator performs poorly for high-rise buildings that are close to neighbouring structures like retaining walls and ramps (i.e., impacts during earthquakes and storms). Earthquakes have been shown to have a negative impact on the seismic performance of fixed-supported buildings, resulting in minor damage or structural failure. However, the possible implications of earthquake-induced poundings on seismically isolated buildings can be far more significant and, therefore, should be evaluated. Here are some practical cases where accounting for pounding is essential:

- In urban locations, structures with differing base isolators may experience varied displacements during earthquakes. Pounding between adjacent buildings might cause damage.
- Poorly built expansion joints can cause pounding on bridges. Pounding might cause damage to the joint or nearby bridge segments.
- High-rise structures with several levels may have varying natural frequencies on each floor. Pounding between floors might happen with significant ground vibrations.
- Vibrations may cause machinery mounted on base isolators to crash with nearby structures or equipment.
- Pounding between structural components, such as beams and columns, can occur when their natural frequencies align.

Many researchers use numerical models to study how pounding can affect the seismic response of isolated buildings (Polycarpou and Komodromos 2010). In addition, tuned mass dampers are also installed at the top layer of the base isolator to enhance their seismic performances. The tuned mass damper uses a mass-dashpot-spring subsystem linked to the isolated superstructure, similar to a

pendulum. The efficiency of the scheme and identifies optimal parameters for designing the tuned mass damper are investigated. The base-isolated structure and the tuned mass damper are both described as linear oscillators with a single-degree-of-freedom each (Taniguchi et al. 2008). Apart from the conventional tuned mass dampers, the tuned mass damper inerters are installed at the isolator mass with ground support (De Angelis et al. 2019) to control the large displacement of the isolation layer during earthquakes (De Domenico and Ricciardi 2018). Instead of the linear tuned mass damper inerter, the nonlinear inerter vibration absorbers are installed in the base-isolated structures with ground attachment to increase their seismic performances and to control their larger base layer displacement during seismic events (Pietrosanti et al. 2021). In addition, in order to lessen these disadvantages, the isolators are attempting to improve their effective mass by utilising inerters (Zhao et al. 2021) and inertial amplifiers (Adhikari and Banerjee 2022) in place of static mass. The classic vibration control devices use an inerter to increase energy dissipation through mass amplification using motion transformers (Papageorgiou et al. 2009). Smith introduced the inerter (Smith and Wang 2004) from the force to the current analogy to reduce structural vibrations (Smith 2002). These inerters have been widely used as vibration control devices in mechanical systems, particularly in vehicles (Swift et al. 2013). An inerter is a mechanical part used in engineering and suspension systems for vehicles (Chowdhury et al. 2023b). It is sometimes referred to as an inertance device or a dynamic vibration absorber (Smith 2020). It was first presented as a possible enhancement for car suspension systems in the early 2000s. The inerter's function is to increase the effective mass of the isolation systems in order to give more damping. An inerter's force is directly proportional to the relative acceleration between its ends, which is one of its most important properties. This implies that more damping is produced by the inerter's force generation (Li et al. 2023), which resists this relative motion. Another efficient mass amplification tool that may raise effective mass and dampen isolation systems is an inertial amplifier. It may also provide the isolators more flexibility and a suitable load-bearing capability at the same time during seismic occurrences. As a result, the isolators' base layer may not sustain any harm, and the isolated structures' lifespan could lengthen. Both inerters and isolators based on inertial amplifiers (Banerjee et al. 2021;

Yilmaz et al. 2007) are suitable for buildings that include nearby features like retaining walls and entrance ramps/entry bridge. However, inertial amplifiers and inerters are generated within the friction bearings' core materials to improve the isolators' performance and serviceability. After taking into account the impact (Chowdhury and Banerjee 2023a) between the building and adjacent structures (i.e., impact designed using "signum" function), the application of inertial amplifiers and inerters to conventional friction bearings/conventional base isolators for mitigating the dynamic responses of the single-degree-of-freedom system (i.e., a conceptualised model of the buildings) with adjacent structures and their corresponding analytical closed-form expressions for optimal design parameters do not exist in the state of the art. In previous studies, many researchers have included and designed dynamic vibration absorbers to avoid pounding with adjacent structures. In addition, the vibration absorbers are installed at the base-isolated structures to increase their seismic performances. However, this approach has several drawbacks. The detailed discussion have already presented in the previous paragraphs. As a result, a research gap is found.

To fill the aforementioned research gap, the inertial amplifier friction bearings and inerter-based friction bearings are introduced in this paper. These novel dampers are applied at the base of the single-degree-of-freedom systems with adjacent structures (i.e., ramp and retaining wall). The impact between the single-degree-of-freedom system and adjacent structures is modelled using the "signum" function. Furthermore, the precise closed-form formulas for the optimum natural frequency and damping ratio of inertial amplifier friction bearing and inerter-based friction bearing are used in single-degree-of-freedom systems with impacting adjacent structures are derived using the H_2 and H_∞ optimisation approach (Roberts and Spanos 2003). Additionally, the dynamic responses of the isolated structures are first acquired via the generation of transfer functions. Later, Newmark-beta method is applied to conduct a numerical study to further validate the results of the frequency domain analysis. In the end, a comparison is made between the dynamic response reduction capabilities of the conventional base isolators and the novel bearings.

STRUCTURAL MODEL

A single-degree-of-freedom system having an adjacent structure isolated by an inertial amplifier

friction bearing has been shown in Figure 1 (a). The adjacent structure is conceptualized as a spring-dashpot and mass system. The distance between the neighbouring structure and the isolated building's base mass is Δ. The base mass, which is stiff in its own plane because of diaphragm action, is believed to be the precise position of the point of contact (shear model of superstructure). Since the system takes no account of rotational degrees of freedom, the impact is normal and not oblique. With neighbouring buildings at the same distance, the effect is taken into account on both sides of the building. It is believed that the superstructure does not move beyond the elastic limit when an earthquake is triggered and an impact occurs. There is just one horizontal component of earthquake ground motion that affects the system. There is no attention given to the impacts of soil-structure interaction. The static mass, damping, and stiffness of the inertial amplifier friction bearing are defined as m_{iv}, c_{iv}, and k_{iv}. The mass and inertial angle of the amplifier are denoted as m_r and θ. After considering the mass amplification effect of the inertial amplifier (Chowdhury and Banerjee 2023b), the effective mass, damping, and stiffness of inertial amplifier friction bearing are derived as

$$m_v = m_{iv} + 0.5 m_r \left(1 + \frac{1}{\tan^2\theta}\right), c_v = 2\xi m_v \varepsilon_v, \quad \text{and} \quad k_v = m_v \varepsilon_v^2 \tag{1}$$

ε_v defines the natural frequency of the inertial amplifier friction bearing. Another single-degree-of-freedom system having an adjacent structure isolated by an inerter-based friction bearing has been shown in Figure 1 (b). The mass of the inerter-based friction bearing is defined as m_v. m_u defines inerter mass. Using this the damping and stiffness of the inerter-based friction bearing have been derived and expressed as

$$c_u = 2\left(m_v + m_u\right)\xi\varepsilon_v \quad \text{and} \quad k_u = \left(m_v + m_u\right)\varepsilon_v^2 \tag{2}$$

μ defines the Poisson's ratio for both isolators. ε_v defines the natural frequency of the inerter-based friction bearing. The conceptualized model of the adjacent structure is shown in Figure 1 (c). k_h and c_h define the stiffness and damping of the retaining wall.

EQUATIONS OF MOTION AND DERIVATIONS OF OPTIMAL DESIGN PARAMETERS

The novel friction bearings are applied to the single-degree-of-freedom systems to control their dynamic responses. The frequency response function is formed using the steady-state responses. Newton's second law is employed to derive the governing equations of motion of the isolated single-degree-of-freedom systems. The isolated single-degree-of-freedom system is subjected to unidirectional base excitation in the horizontal direction. Due to that, an impact occurs between the isolated single-degree-of-freedom system and the retaining wall when the relative displacement of the bearing exceeds the relative distance between the retaining wall and the bearing mass. The retaining wall is conceptualised as a spring, dash-pot model. After considering these conceptualisations, the impact is analytically formulated by the "signum" function instead of other existing impact models, such as the Hertzian model (Balachandran 2003) which is mathematically formulated by considering many assumptions. In some cases, the equivalent viscous damping is used to represent inelastic impacts in earthquake pounding situations (Anagnostopoulos 2004). The "signum" function allows us to derive analytical optimal closed-form solutions for the design parameters of these upgraded base isolators for the impacting dynamic systems which can not be achieved using the Hertzian model. In addition, the direct numerical solver needs to be used to solve the Hertzian model (Davies and Balachandran 2000). For some cases, the Hertzian model fits better experimental studies of pounding between different materials. The analytical optimisation methods are not applicable for Hertzian contact model-related base-isolated impacting dynamic systems. Therefore, the "signum" function is more accurate and feasible than the Hertzian model for formulating the impact in terms of analytical solutions.

Inertial amplifier friction bearing

The governing equations of motion for the single-degree-of-freedom systems isolated by the inertial amplifier friction bearing have been derived as

$$\begin{aligned} &m\ddot{w}_s + m\ddot{w}_b + c\dot{w}_s + kw_s = -m\ddot{w}_g \\ &m_v\ddot{w}_b + c_v\dot{w}_b + k_v w_b + \mu m_v g\,\mathrm{sgn}(\dot{w}_b) - c\dot{w}_s - kw_s + k_h\left(|w_b| - \delta\right)\mathrm{sgn}(w_b) + c_h\dot{w}_b = -m_v\ddot{w}_g \end{aligned} \tag{3}$$

where w_s and w_b define the relative displacement of the single-degree-of-freedom system and isolator. The above equation is a highly nonlinear equation. To derive optimal design parameters for inertial amplifier friction bearing analytically, Eq. (3) needs to be linearised. Therefore, the statistical linearisation method is employed for Eq. (3), and the linearised element of the nonlinear element is derived as

$$\begin{aligned} c_{ve} &= E\left\{\frac{\mathrm{d}(\mu m_v g\,\mathrm{sgn}(\dot{w}_b))}{\mathrm{d}\dot{w}_b}\right\} = \sqrt{\frac{2}{\pi}}\frac{\mu m_v g}{\sigma_{\dot{w}_b}} \\ \text{and} \quad k_{ve} &= E\left\{\frac{d(k_h\delta\,\mathrm{sgn}(w_b))}{\mathrm{d}w_b}\right\} = \sqrt{\frac{2}{\pi}}\frac{k_h\delta}{\sigma_{w_b}} \end{aligned} \tag{4}$$

where δ defines the relative distance between the adjacent structure and isolator mass. Eq. (4) is applied to Eq. (3) and the second expression of Eq. (3) is modified as

$$\begin{aligned} m_v\ddot{w}_b + c_v\dot{w}_b + k_v w_b + c_{ve}\dot{w}_b - c\dot{w}_s \\ -kw_s + k_h w_b - k_{ve} w_b + c_h\dot{w}_b \end{aligned} = -m_v\ddot{w}_g \tag{5}$$

The steady-state solutions are considered as $w_s = W_s e^{\mathrm{i}\varepsilon t}$, $w_b = W_b e^{\mathrm{i}\varepsilon t}$, and $\ddot{w}_g = W_g e^{\mathrm{i}\varepsilon t}$. The steady-state solutions are applied to Eq. (3), and the frequency response function has been derived

as

$$\begin{bmatrix} 2\,\zeta\,\varepsilon_s\,y + y^2 + {\varepsilon_s}^2 & y^2 \\ -2\,\zeta\,\varepsilon_s\,y - {\varepsilon_s}^2 & B_{22} \end{bmatrix} \begin{Bmatrix} W_s \\ W_b \end{Bmatrix} = -\begin{bmatrix} 1 \\ \gamma_v \end{bmatrix} W_g \tag{6}$$

$$B_{22} = 2\,\xi\,y\gamma_v\,\varepsilon_v + 2\,\zeta\,\varepsilon_s\,y + \kappa\,{\varepsilon_s}^2 + \gamma_v\,y^2 + \gamma_v\,{\varepsilon_v}^2 + c_{ve}\,y - k_{ve}\,\delta$$

where $y = \mathrm{i}\varepsilon$. The dynamic response of the single-degree-of-freedom system is derived as

$$H_s(y) = \left(\frac{W_s}{W_g}\right)(y) = \frac{-2\,\xi\,y\gamma_v\,\varepsilon_v - 2\,\zeta\,\varepsilon_s\,y - \kappa\,{\varepsilon_s}^2 - \gamma_v\,{\varepsilon_v}^2 - c_{ve}\,y + k_{ve}\,\delta}{\Phi} \tag{7}$$

The dynamic response of the isolator is derived as

$$H_b(y) = \left(\frac{W_b}{W_g}\right)(y) = \frac{-2\,\zeta\,y\gamma_v\,\varepsilon_s - 2\,\zeta\,\varepsilon_s\,y - \gamma_v\,y^2 - \gamma_v\,{\varepsilon_s}^2 - {\varepsilon_s}^2}{\Phi} \tag{8}$$

The denominator Φ is derived as

$$\begin{aligned} \Phi = {} & y^4\gamma_v + (2\,\zeta\,\gamma_v\,\varepsilon_s + 2\,\xi\,\varepsilon_v\,\gamma_v + 4\,\zeta\,\varepsilon_s + c_{ve})\,y^3 \\ & + \begin{pmatrix} 4\,\zeta\,\varepsilon_s\,\xi\,\varepsilon_v\,\gamma_v + 4\,\zeta^2{\varepsilon_s}^2 + 2\,\zeta\,\varepsilon_s\,c_{ve} \\ +\kappa\,{\varepsilon_s}^2 + \gamma_v\,{\varepsilon_s}^2 + \gamma_v\,{\varepsilon_v}^2 - k_{ve}\,\delta + {\varepsilon_s}^2 \end{pmatrix} y^2 \\ & + \begin{pmatrix} 2\,\zeta\,\kappa\,{\varepsilon_s}^3 + 2\,\zeta\,\gamma_v\,\varepsilon_s\,{\varepsilon_v}^2 + 2\,\xi\,\gamma_v\,{\varepsilon_s}^2\varepsilon_v \\ -2\,\zeta\,\delta\,k_{ve}\,\varepsilon_s + 2\,\zeta\,{\varepsilon_s}^3 + c_{ve}\,{\varepsilon_s}^2 \end{pmatrix} y \\ & +\kappa\,{\varepsilon_s}^4 + \gamma_v\,{\varepsilon_s}^2{\varepsilon_v}^2 - \delta\,k_{ve}\,{\varepsilon_s}^2 \end{aligned} \tag{9}$$

Equation (7) and Eq. (9) are further applied to derive the exact closed-form expression for the optimal design parameters of the inertial amplifier friction bearing using H_2 and H_∞ optimisation methods. c_{ve} and k_{ve} define the equivalent damping and stiffness of the isolator and the retaining wall. To conduct the analytical optimisation procedure, two initial conditions have been derived, i.e. $\zeta = 0$, $\sigma_{\dot{w}_b} = 0$, and $\sigma_{w_b} = 0$. These initial conditions are applied to Eq. (7) and Eq. (9). Accordingly, these equations are re-derived and applied for the optimisation procedures.

H_2 optimisation

Equation (7) and Eq. (9) with the derived initial conditions are applied to perform the H_2 optimisation procedure (Chowdhury et al. 2022). In addition, the random white noise excitation (Roberts and Spanos 2003) is loaded at the base of the isolated single-degree-of-freedom system to avail the H_2 optimisation method (Chowdhury and Banerjee 2024). Accordingly, the standard deviation of the displacement of the single-degree-of-freedom system derives as

$$\sigma_{w_s}^2 = \frac{S_0\pi\left(4\gamma_v^2\varepsilon_v^2\varepsilon_s^2\xi^2 + \kappa^2\varepsilon_s^4 + 2\gamma_v\varepsilon_v^2\varepsilon_s^2\kappa + \gamma_v^2\varepsilon_v^4 + \kappa\,\varepsilon_s^4 + \gamma_v\varepsilon_v^2\varepsilon_s^2\right)}{2\varepsilon_v\gamma_v\xi\,\varepsilon_s^6} \tag{10}$$

To derive the accurate closed-form formula for the best design parameters, Eq. (10) has been partially differentiated with regard to the damping ratio ξ and frequency ε_v of the innovative isolators. Consequently, by minimising $\sigma_{w_s}^2$, these optimal design parameters have been found, which results in

$$\frac{\partial\sigma_{w_s}^2}{\partial\xi} = 0 \quad \text{and} \quad \frac{\partial\sigma_{w_s}^2}{\partial\varepsilon_v} = 0 \tag{11}$$

Eq. (10) has been added to Eq. (11)'s first equation. Consequently, the new isolators' optimal damping ratio has been determined to be

$$\xi = \frac{\sqrt{\kappa^2{\varepsilon_s}^4 + 2\,\kappa\,\gamma_v\,{\varepsilon_s}^2{\varepsilon_v}^2 + {\gamma_v}^2{\varepsilon_v}^4 + \kappa\,{\varepsilon_s}^4 + \gamma_v\,{\varepsilon_s}^2{\varepsilon_v}^2}}{2\varepsilon_v\,\varepsilon_s\,\gamma_v} \tag{12}$$

The optimal damping ratio of the new isolators is defined as Equation (12). The frequency of the new isolators ε_v is contained in this closed-form calculation and must be separated. Eq. (12) has been replaced in Eq. (10) in order to accomplish that. Currently, $\sigma_{w_s}^2$ is stated as changed.

$$\sigma_{w_s}^2 = \frac{2S_0\sqrt{\left((\kappa+1)\,{\varepsilon_s}^2 + \gamma_v\,{\varepsilon_v}^2\right)\left(\kappa\,{\varepsilon_s}^2 + \gamma_v\,{\varepsilon_v}^2\right)}\pi}{{\varepsilon_s}^5} \tag{13}$$

To determine the optimal frequency value of innovative isolators ε_v, Equation (13) has been introduced into the second constraints of Eq. (11). Consequently, the new isolators' optimal frequency has been determined to be

$$(\varepsilon_v)_{\text{opt}} = \frac{\sqrt{2\,\gamma_v\ (2\,\kappa+1)}\varepsilon_s}{2\gamma_v} \tag{14}$$

The frequency ratio of the isolator is derived using Eq. (14) and expressed as

$$(\alpha_v)_{\text{opt}} = \frac{\sqrt{2\,\gamma_v\ (2\,\kappa+1)}}{2\gamma_v} \tag{15}$$

In Eq. (12), Equation (14) has been replaced. Consequently, the new isolators' optimal damping ratio has been determined to be

$$(\xi)_{\text{opt}} = \frac{\sqrt{{\varepsilon_s}^4\left(16\,\kappa^2+16\,\kappa+3\right)}\sqrt{2}}{4\sqrt{2\,\gamma_v\,\kappa+\gamma_v}{\varepsilon_s}^2} \tag{16}$$

Figure 2 (a) and (b) depict the changes in the optimal frequency and damping ratios in relation to the isolator mass ratio of inertial amplifier friction bearing for various inertial angle values. As the isolator mass ratio rises, the optimal frequency and damping ratios decrease. As the inertial angle rises, the optimal frequency and damping ratios increase. The displacement response of the isolator's standard deviation has been determined to be

$$\sigma_{w_b}^2 = \frac{\pi\,S_0\left(\left({\gamma_v}^2+\kappa+2\,\gamma_v+1\right){\varepsilon_s}^2+\gamma_v\,{\varepsilon_v}^2\right)}{2\xi\,\gamma_v\,{\varepsilon_s}^2\varepsilon_v\ \left(\kappa\,{\varepsilon_s}^2+\gamma_v\,{\varepsilon_v}^2\right)} \tag{17}$$

The velocity response of the isolator's standard deviation has been determined to be

$$\sigma_{\dot{w}_b}^2 = \frac{(\gamma_v+1)\,\pi\,S_0}{2\xi\,\gamma_v\,\varepsilon_v} \tag{18}$$

Further, the optimal design parameters are derived using the H_∞ optimisation method.

H_∞ optimisation

The non-dimensional form of Eq. (6) with the initial conditions is applied to conduct the H_∞ optimisation method. In addition, it has been considered that the isolated structure is subjected harmonic base excitation. Hence, the non-dimentional form of the frequency response function is derived and expressed as

$$\begin{bmatrix} -\alpha^2+1 & -\alpha^2 \\ -1 & -\gamma_v\alpha^2 + 2\,\mathrm{i}\xi\alpha_v\gamma_v\alpha + \gamma_v\alpha_v^2 + \kappa \end{bmatrix} \begin{Bmatrix} W_s \\ W_b \end{Bmatrix} = -\begin{bmatrix} 1 \\ \gamma_v \end{bmatrix} \frac{W_g}{\varepsilon_s^2} \tag{19}$$

The dynamic response of the single-degree-of-freedom system is derived as

$$H_s(\alpha) = \left(\frac{W_s}{W_g}\right)\varepsilon_s^2 = \frac{\gamma_v\alpha_v^2 + \kappa + 2\,\mathrm{i}\xi\alpha_v\gamma_v\alpha}{\Phi} \tag{20}$$

The dynamic response of the isolator is derived as

$$H_b(\alpha) = \left(\frac{W_b}{W_g}\right)\varepsilon_s^2 = \frac{-\gamma_v\alpha^2 + \gamma_v + 1}{\Phi} \tag{21}$$

The denominator of Eq. (20) and Eq. (21) is derived as

$$\Phi = -\alpha^4\gamma_v + \alpha^2\alpha_v^2\gamma_v + \alpha^2\kappa + \gamma_v\alpha^2 - \gamma_v\alpha_v^2 + \alpha^2 - \kappa + \mathrm{i}\left(2\alpha^3\xi\alpha_v\gamma_v - 2\xi\alpha_v\gamma_v\alpha\right) \tag{22}$$

The resultant of Eq. (20) is derived to generate constraints for H_∞ optimisation procedure and expressed as follows.

$$|H_s(\alpha)| = \sqrt{\frac{W_1^2 + \xi^2 W_2^2}{W_3^2 + \xi^2 W_4^2}} = \left|\frac{W_2}{W_4}\right| \sqrt{\frac{\frac{W_1^2}{W_2^2} + \xi^2}{\frac{W_3^2}{W_4^2} + \xi^2}} \tag{23}$$

Two constraints are derived from Eq. (23) using the fixed-point theory and expressed as

$$\left|\frac{W_1}{W_2}\right|_{\alpha_j} = \left|\frac{W_3}{W_4}\right|_{\alpha_j} \quad \text{and} \quad \left|\frac{W_2}{W_4}\right|_{\alpha_1} = \left|\frac{W_2}{W_4}\right|_{\alpha_2} \tag{24}$$

286 $W_{j=1,2,3,4}$ has been derived as

$$\begin{aligned} W_1 = \alpha_v^2\gamma_v + \kappa, W_2 = 2\alpha_v\gamma_v\alpha, W_4 = 2\alpha^3\alpha_v\gamma_v - 2\alpha_v\gamma_v\alpha, \\ \text{and} \quad W_3 = -\alpha^4\gamma_v + \alpha^2\alpha_v^2\gamma_v + \alpha^2\kappa + \gamma_v\alpha^2 - \alpha_v^2\gamma_v + \alpha^2 - \kappa \end{aligned} \tag{25}$$

288 Equation (25) is substituted in the first expression of the Eq. (24).

$$\alpha^4\gamma_v + \left(-2\gamma_v\alpha_v^2 - 2\kappa - \gamma_v - 1\right)\alpha^2 + 2\gamma_v\alpha_v^2 + 2\kappa = 0 \tag{26}$$

290 Equation (26) is written as

$$\alpha^4 + \left(-\alpha_1^2 - \alpha_2^2\right)\alpha^2 + \alpha_1^2\alpha_2^2 = 0 \tag{27}$$

292 The summation of the two roots, i.e. $\alpha_1^2 + \alpha_2^2$, are derived after comparing Eq. (26) and Eq. (27).

$$\alpha_1^2 + \alpha_2^2 = \frac{2\gamma_v\alpha_v^2 + 2\kappa + \gamma_v + 1}{\gamma_v} \tag{28}$$

294 Equation (25) is substituted in the second expression of the Eq. (24).

$$\alpha_1^2 + \alpha_2^2 = 2 \tag{29}$$

296 Equation (28) and Eq. (29) are equating to derive the mathematical expression for the optimal
297 natural frequency of the isolator.

$$(\alpha_v)_{\text{opt}} = \frac{\sqrt{2\gamma_v^2 - 4\gamma_v\kappa - 2\gamma_v}}{2\gamma_v} \tag{30}$$

Equation (23) is squared and partially differentiated with respect to the damping ratio of the isolator to derive its optimal value and the mathematical expression is derived as

$$\left.\frac{\partial |H_s(\alpha)|^2}{\partial \alpha^2}\right|_{\alpha_{1,2}^2} = 0 \quad \text{and} \quad (\xi)_{\text{opt}} = \sqrt{\frac{\xi_1^2 + \xi_2^2}{2}} \tag{31}$$

Applying the first expression of Eq. (31), the optimal damping ratio is derived as

$$\begin{aligned}
&A_1\xi^4 + A_2\xi^2 + A_3 = 0,\\
&A_1 = -32\alpha_{1,2}^4\alpha_\nu^4\gamma_\nu^4\left(\alpha_{1,2}^2 - 1\right),\\
&A_2 = \begin{array}{c} -12\alpha_{1,2}^8\alpha_\nu^2\gamma_\nu^4 + \left(16\alpha_\nu^4\gamma_\nu^4 + 16\kappa\,\alpha_\nu^2\gamma_\nu^3 + 16\alpha_\nu^2\gamma_\nu^4 + 16\alpha_\nu^2\gamma_\nu^3\right)\alpha_{1,2}^6 \\ +\left(\begin{array}{c} -16\alpha_\nu^6\gamma_\nu^4 - 32\kappa\,\alpha_\nu^4\gamma_\nu^3 - 16\alpha_\nu^4\gamma_\nu^4 - 8\alpha_\nu^4\gamma_\nu^3 - 16\kappa^2\alpha_\nu^2\gamma_\nu^2 \\ -16\kappa\,\alpha_\nu^2\gamma_\nu^3 - 4\alpha_\nu^2\gamma_\nu^4 - 8\kappa\,\alpha_\nu^2\gamma_\nu^2 - 8\alpha_\nu^2\gamma_\nu^3 - 4\alpha_\nu^2\gamma_\nu^2 \end{array}\right)\alpha_{1,2}^4 \\ +\left(16\alpha_\nu^6\gamma_\nu^4 + 32\kappa\,\alpha_\nu^4\gamma_\nu^3 + 16\kappa^2\alpha_\nu^2\gamma_\nu^2\right)\alpha_{1,2}^2 \end{array},\\
&A_3 = \begin{array}{c} \left(-4\alpha_\nu^4\gamma_\nu^4 - 8\kappa\,\alpha_\nu^2\gamma_\nu^3 - 4\kappa^2\gamma_\nu^2\right)\alpha_{1,2}^6 \\ +\left(\begin{array}{c} 6\alpha_\nu^6\gamma_\nu^4 + 18\kappa\,\alpha_\nu^4\gamma_\nu^3 + 6\alpha_\nu^4\gamma_\nu^4 + 6\alpha_\nu^4\gamma_\nu^3 + 18\kappa^2\alpha_\nu^2\gamma_\nu^2 + 12\kappa\,\alpha_\nu^2\gamma_\nu^3 \\ +12\kappa\,\alpha_\nu^2\gamma_\nu^2 + 6\kappa^3\gamma_\nu + 6\kappa^2\gamma_\nu^2 + 6\kappa^2\gamma_\nu \end{array}\right)\alpha_{1,2}^4 \\ +\left(\begin{array}{c} -2\alpha_\nu^8\gamma_\nu^4 - 8\kappa\,\alpha_\nu^6\gamma_\nu^3 - 8\alpha_\nu^6\gamma_\nu^4 - 4\alpha_\nu^6\gamma_\nu^3 - 12\kappa^2\alpha_\nu^4\gamma_\nu^2 - 24\kappa\,\alpha_\nu^4\gamma_\nu^3 \\ -2\alpha_\nu^4\gamma_\nu^4 - 12\kappa\,\alpha_\nu^4\gamma_\nu^2 - 4\alpha_\nu^4\gamma_\nu^3 - 8\kappa^3\alpha_\nu^2\gamma_\nu - 24\kappa^2\alpha_\nu^2\gamma_\nu^2 \\ -4\kappa\,\alpha_\nu^2\gamma_\nu^3 - 2\alpha_\nu^4\gamma_\nu^2 - 12\kappa^2\alpha_\nu^2\gamma_\nu - 8\kappa\,\alpha_\nu^2\gamma_\nu^2 - 2\kappa^4 - 8\kappa^3\gamma_\nu \\ -2\kappa^2\gamma_\nu^2 - 4\kappa\,\alpha_\nu^2\gamma_\nu - 4\kappa^3 - 4\kappa^2\gamma_\nu - 2\kappa^2 \end{array}\right)\alpha_{1,2}^2 \\ +2\alpha_\nu^8\gamma_\nu^4 + 8\kappa\,\alpha_\nu^6\gamma_\nu^3 + 2\alpha_\nu^6\gamma_\nu^4 + 2\alpha_\nu^6\gamma_\nu^3 + 12\kappa^2\alpha_\nu^4\gamma_\nu^2 + 6\kappa\,\alpha_\nu^4\gamma_\nu^3 \\ +6\kappa\,\alpha_\nu^4\gamma_\nu^2 + 8\kappa^3\alpha_\nu^2\gamma_\nu + 6\kappa^2\alpha_\nu^2\gamma_\nu^2 + 6\kappa^2\alpha_\nu^2\gamma_\nu + 2\kappa^4 + 2\kappa^3\gamma_\nu + 2\kappa^3 \end{array},\\
&\xi_{1,2}^2 = \frac{-A_2 \pm \sqrt{A_2^2 - 4A_1A_3}}{2A_1}
\end{aligned} \tag{32}$$

where α_1^2 and α_2^2 are the individual root of the Eq. (26). The value of $\alpha_1^2 + \alpha_2^2$ from Eq. (29) has been substituted in Eq. (26) before deriving the exact closed-form expression for each root, i.e. α_1^2

and α_2^2. As a result, the exact closed-form expressions for for α_1^2 and α_2^2 is derived as

$$\alpha_{1,2}^2 = \frac{\gamma_v \pm \sqrt{-2\alpha_v^2\gamma_v^2 - 2\kappa\gamma_v + \gamma_v^2}}{\gamma_v} \tag{33}$$

Equation (30) is substituted in Eq. (33) to obtain the optimal closed-form solutions for Eq. (33).

$$\left(\alpha_{1,2}\right)_{\text{opt}}^2 = \frac{\sqrt{\gamma_v} \pm 1}{\sqrt{\gamma_v}} \tag{34}$$

Equation (30) and Eq. (34) are substituted in Eq. (32). Accordingly, the optimal closed-form solution for the damping ratio of the isolator is derived as

$$\begin{aligned}
(\xi)_{\text{opt}} &= \sqrt{\frac{\begin{array}{l} 2\gamma_v^4\kappa - \gamma_v^5 - 10\gamma_v^3\kappa + 6\gamma_v^4 + 14\gamma_v^2\kappa - Q_1\gamma_v^{\frac{3}{2}} + Q_2\gamma_v^{\frac{3}{2}} - 12\gamma_v^3 \\ -6\gamma_v\kappa - \sqrt{\gamma_v}\,Q_1 + 2Q_1\gamma_v + Q_2\sqrt{\gamma_v} + 2Q_2\gamma_v + 10\gamma_v^2 - 3\gamma_v \end{array}}{8\gamma_v\left(\sqrt{\gamma_v}+1\right)^2\left(2\kappa-\gamma_v+1\right)^2\left(\sqrt{\gamma_v}-1\right)^2}} \\
Q_1 &= \sqrt{\left(\sqrt{\gamma_v}+1\right)^4\gamma_v\left(\sqrt{\gamma_v}-1\right)^2\left(2\kappa-\gamma_v+1\right)^2} \\
Q_2 &= \sqrt{\left(\sqrt{\gamma_v}+1\right)^2\gamma_v\left(\sqrt{\gamma_v}-1\right)^4\left(2\kappa-\gamma_v+1\right)^2}
\end{aligned} \tag{35}$$

The variations of optimal frequency and damping ratios are H_∞ optimised friction bearings are shown in Figure 3 (a) and Figure 3 (b). The optimal frequency ratios are lowered when the isolator mass ratio increases. The frequency ratios decrease with a certain range when the amplifier angle increases. The amplifier angle varies from 5^o to 15^o as after 12^o, the damping ratio crosses 1.0. This amount of damping ratio is not economical for construction purposes. To achieve a cost-effective robust design from the H_∞ optimised isolator, the amplifier angle should be less than equal to 12^o, i.e. $\theta \leq 12^o$. The relationship between the amplifier angle and isolator mass ratio determines the optimal frequency and damping ratios.

Inerter-based friction bearing

The governing equations of motion of the single-degree-of-freedom systems isolated by the inerter-based friction bearing are derived using Newton's law and expressed as

$$\begin{aligned} & m\ddot{w}_s + m\ddot{w}_b + c\dot{w}_s + kw_s = -m\ddot{w}_g \\ & m_v\ddot{w}_b + m_u\ddot{w}_b + c_u\dot{w}_b + k_u w_b + \mu\left(m_u + m_v\right) g\,\mathrm{sgn}(\dot{w}_b) \\ & \quad -c\dot{w}_s - kw_s + k_h\left(|w_b| - \delta\right)\mathrm{sgn}(w_b) + c_h\dot{w}_b \end{aligned} = -m_v\ddot{w}_g \tag{36}$$

where w_s and w_b define the relative displacement of the single-degree-of-freedom system and isolator, and δ defines the relative distance between the adjacent structure and isolator mass. It is extremely nonlinear to solve the problem above. Eq. (36) must be linearised to calculate the optimal design parameters for inerter-based friction bearing analytically. As a result, for Eq. (36), the statistical linearisation approach is used, and the linearised element of the nonlinear element is obtained as

$$\begin{aligned} c_{ue} = E\left\{\frac{\mathrm{d}(\mu(m_v + m_u)g\,\mathrm{sgn}(\dot{w}_b))}{\mathrm{d}\dot{w}_b}\right\} = \sqrt{\frac{2}{\pi}}\frac{\mu(m_v + m_u)g}{\sigma_{\dot{w}_b}} \\ \text{and} \quad k_{ue} = E\left\{\frac{d(k_h\delta\,\mathrm{sgn}(w_b))}{\mathrm{d}w_b}\right\} = \sqrt{\frac{2}{\pi}}\frac{k_h\delta}{\sigma_{w_b}} \end{aligned} \tag{37}$$

After applying Equation (37) to Eq. (36), Eq. (36)'s second expression is changed to

$$\begin{aligned} & m_v\ddot{w}_b + m_u\ddot{w}_b + c_u\dot{w}_b + k_u w_b + c_{ue}\dot{w}_b \\ & \quad -c\dot{w}_s - kw_s + k_h w_b - k_{ue} w_b + c_h\dot{w}_b \end{aligned} = -m_v\ddot{w}_g \tag{38}$$

$w_s = W_s e^{i\varepsilon t}$, $w_b = W_b e^{i\varepsilon t}$, and $\ddot{w}_g = W_g e^{i\varepsilon t}$ are the steady-state solutions. After applying the steady-state solutions to Eq. (36), the frequency response function may be found as

$$\begin{bmatrix} 2\zeta\,\varepsilon_s\,y + y^2 + {\varepsilon_s}^2 & y^2 \\ -2\zeta\,\varepsilon_s\,y - {\varepsilon_s}^2 & B_{22} \end{bmatrix} \begin{Bmatrix} W_s \\ W_b \end{Bmatrix} = -\begin{bmatrix} 1 \\ \gamma_v \end{bmatrix} W_g \tag{39}$$

$$B_{22} = \begin{array}{c} (\gamma_v + \gamma_u)\,y^2 + 2\zeta\,\varepsilon_s\,y + c_{ue}\,y + 2\xi\,\varepsilon_v\,(\gamma_v + \gamma_u)\,y \\ -k_{ue}\,\delta + {\varepsilon_s}^2\kappa + (\gamma_v + \gamma_u)\,{\varepsilon_v}^2 \end{array}$$

where $y = i\varepsilon$. The dynamic response of the single-degree-of-freedom system is derived as

$$H_s(y) = \left(\frac{W_s}{W_g}\right)(y) = \frac{\begin{array}{c} -2\xi\,\varepsilon_v\,y\gamma_u - 2\xi\,\varepsilon_v\,y\gamma_v - 2\zeta\,\varepsilon_s\,y - {\varepsilon_s}^2\kappa \\ -y^2\gamma_u - {\varepsilon_v}^2\gamma_u - {\varepsilon_v}^2\gamma_v - c_{ue}\,y + k_{ue}\,\delta \end{array}}{\Phi} \tag{40}$$

The dynamic response of the isolator is derived as

$$H_b(y) = \left(\frac{W_b}{W_g}\right)(y) = \frac{-2\zeta\,y\gamma_v\,\varepsilon_s - 2\zeta\,\varepsilon_s\,y - y^2\gamma_v - \gamma_v\,{\varepsilon_s}^2 - {\varepsilon_s}^2}{\Phi} \tag{41}$$

The denominator Φ is derived as

$$\Phi = \begin{array}{c} (\gamma_v + \gamma_u)\,y^4 \\ +\left(\begin{array}{c} 2\zeta\,\varepsilon_s\,\gamma_u + 2\zeta\,\varepsilon_s\,\gamma_v + 2\xi\,\varepsilon_v\,\gamma_u + 2\xi\,\varepsilon_v\,\gamma_v + 4\zeta\,\varepsilon_s + c_{ue} \end{array}\right) y^3 \\ +\left(\begin{array}{c} 4\zeta\,\varepsilon_s\,\xi\,\varepsilon_v\,\gamma_u + 4\zeta\,\varepsilon_s\,\xi\,\varepsilon_v\,\gamma_v + 4\zeta^2{\varepsilon_s}^2 + 2\zeta\,\varepsilon_s\,c_{ue} \\ +{\varepsilon_s}^2\kappa + \gamma_u\,{\varepsilon_s}^2 + {\varepsilon_v}^2\gamma_u + \gamma_v\,{\varepsilon_s}^2 + {\varepsilon_v}^2\gamma_v - k_{ue}\,\delta + {\varepsilon_s}^2 \end{array}\right) y^2 \\ +\left(\begin{array}{c} 2\zeta\,\kappa\,{\varepsilon_s}^3 + 2\zeta\,\gamma_u\,\varepsilon_s\,{\varepsilon_v}^2 + 2\zeta\,\gamma_v\,\varepsilon_s\,{\varepsilon_v}^2 + 2\xi\,\gamma_u\,{\varepsilon_s}^2\varepsilon_v \\ +2\xi\,\gamma_v\,{\varepsilon_s}^2\varepsilon_v - 2\zeta\,\delta\,k_{ue}\,\varepsilon_s + 2\zeta\,{\varepsilon_s}^3 + c_{ue}\,{\varepsilon_s}^2 \end{array}\right) y \\ +\kappa\,{\varepsilon_s}^4 + \gamma_u\,{\varepsilon_s}^2{\varepsilon_v}^2 + \gamma_v\,{\varepsilon_s}^2{\varepsilon_v}^2 - \delta\,k_{ue}\,{\varepsilon_s}^2 \end{array} \tag{42}$$

Equation (40) and Eq. (42) are further applied to derive the exact closed-form expression for the optimal design parameters of the inerter-based friction bearing using H_2 and H_∞ optimisation

methods. c_{ue} and k_{ue} define the equivalent damping and stiffness of the isolator and the retaining wall. To conduct the analytical optimisation procedure, two initial conditions have been derived, i.e. $\zeta = 0$, $\sigma_{\dot{w}_b} = 0$, and $\sigma_{w_b} = 0$. These initial conditions are applied to Eq. (40) and Eq. (42). Accordingly, these equations are re-derived and applied for the optimisation procedures.

H_2 optimisation

Equation (40) and Eq. (42) with the derived initial conditions are applied to perform the H_2 optimisation procedure. In addition, the random white noise excitation (Roberts and Spanos 2003) is loaded at the base of the isolated single-degree-of-freedom system to avail the H_2 optimisation method (Chowdhury and Banerjee 2024). Accordingly, the standard deviation of the displacement of the single-degree-of-freedom system derives as

$$\sigma_{w_s}^2 = \frac{\pi S_0 \left(\begin{array}{c} 4\,\varepsilon_v{}^2\varepsilon_s{}^2\gamma_u{}^2\xi^2 + 8\,\varepsilon_v{}^2\varepsilon_s{}^2\gamma_v\,\gamma_u\,\xi^2 + 4\,\varepsilon_v{}^2\varepsilon_s{}^2\xi^2\gamma_v{}^2 \\ +\varepsilon_s{}^4\kappa^2 - 2\,\varepsilon_s{}^4\gamma_u\,\kappa + 2\,\varepsilon_v{}^2\varepsilon_s{}^2\gamma_u\,\kappa \\ +2\,\varepsilon_v{}^2\varepsilon_s{}^2\gamma_v\,\kappa + \varepsilon_s{}^4\gamma_u{}^2 - 2\,\varepsilon_v{}^2\varepsilon_s{}^2\gamma_u{}^2 \\ +\gamma_u{}^2\varepsilon_v{}^4 - 2\,\varepsilon_v{}^2\varepsilon_s{}^2\gamma_v\,\gamma_u + 2\,\gamma_u\,\gamma_v\,\varepsilon_v{}^4 \\ +\gamma_v{}^2\varepsilon_v{}^4 + \varepsilon_s{}^4\kappa + \varepsilon_v{}^2\varepsilon_s{}^2\gamma_u + \varepsilon_v{}^2\varepsilon_s{}^2\gamma_v \end{array} \right)}{2\,\varepsilon_v\,\xi\,\left(\gamma_v + \gamma_u\right)\varepsilon_s{}^6} \tag{43}$$

Eq. (43) has been partially differentiated concerning the damping ratio ξ and frequency ε_v of the novel isolators to get the precise closed-form formula for the optimal design parameters. Consequently, these optimal design parameters have been obtained by minimising $\sigma_{w_s}^2$. This leads to

$$\frac{\partial \sigma_{w_s}^2}{\partial \xi} = 0 \quad \text{and} \quad \frac{\partial \sigma_{w_s}^2}{\partial \varepsilon_v} = 0 \tag{44}$$

The first equation for Eq. (44) now includes Eq. (43). As a result, the optimal damping ratio for the new isolators is found to be

$$\xi = \sqrt{\frac{2\ (\kappa - \gamma_u + 1/2)\ (\gamma_u + \gamma_v)\ {\varepsilon_v}^2 {\varepsilon_s}^2 + {\varepsilon_v}^4\ (\gamma_u + \gamma_v)^2 - \left(-\kappa^2 + 2\,\kappa\,\gamma_u - {\gamma_u}^2 - \kappa\right) {\varepsilon_s}^4}{4\,{\varepsilon_s}^2 {\varepsilon_v}^2\ (\gamma_u + \gamma_v)^2}} \tag{45}$$

Equation (45) is the optimal damping ratio of the new isolators. This closed-form computation contains the frequency of the new isolators ε_v, which needs to be separated. To do that, Eq. (43) has taken the place of Eq. (45). At now, $\sigma_{w_s}^2$ is expressed as altered.

$$\sigma_{w_s}^2 = \frac{2\,S_0\pi \left(\begin{array}{c} \kappa^2 {\varepsilon_s}^4 - 2\,\kappa\,\gamma_u\,{\varepsilon_s}^4 + 2\,\kappa\,\gamma_u\,{\varepsilon_s}^2{\varepsilon_v}^2 + 2\,\kappa\,\gamma_v\,{\varepsilon_s}^2{\varepsilon_v}^2 \\ +{\gamma_u}^2{\varepsilon_s}^4 - 2\,{\gamma_u}^2{\varepsilon_s}^2{\varepsilon_v}^2 + {\gamma_u}^2{\varepsilon_v}^4 - 2\,\gamma_u\,\gamma_v\,{\varepsilon_s}^2{\varepsilon_v}^2 \\ +2\,\gamma_u\,\gamma_v\,{\varepsilon_v}^4 + {\gamma_v}^2{\varepsilon_v}^4 + \kappa\,{\varepsilon_s}^4 + \gamma_u\,{\varepsilon_s}^2{\varepsilon_v}^2 + \gamma_v\,{\varepsilon_s}^2{\varepsilon_v}^2 \end{array} \right)}{G_1 \varepsilon_v\ (\gamma_u + \gamma_v)\ {\varepsilon_s}^6} \tag{46}$$

$$G_1 = \sqrt{\frac{\left(\kappa^2 - 2\,\kappa\,\gamma_u + {\gamma_u}^2 + \kappa\right) {\varepsilon_s}^4 + 2\,{\varepsilon_v}^2\ (\gamma_u + \gamma_v)\ (\kappa - \gamma_u + 1/2)\ {\varepsilon_s}^2 + {\varepsilon_v}^4\ (\gamma_u + \gamma_v)^2}{{\varepsilon_s}^2 {\varepsilon_v}^2\ (\gamma_u + \gamma_v)^2}}$$

In the second constraint of Eq. (44), Equation (46) has been incorporated to find the optimal frequency value of novel isolators ε_v. As a result, the optimal frequency for the new isolators is found to be

$$(\varepsilon_v)_{\text{opt}} = \frac{\sqrt{2}\sqrt{(\gamma_u + \gamma_v)\ (2\,\kappa - 2\,\gamma_u + 1)}\varepsilon_s}{2\,\gamma_u + 2\,\gamma_v} \tag{47}$$

Equation (47) has been substituted in Eq. (45). As a result, the optimal damping ratio for the new isolators is found to be

$$(\xi)_{\text{opt}} = \frac{\sqrt{2}\sqrt{\frac{16\,{\gamma_u}^2 + (-32\,\kappa - 12)\gamma_u + 16\,\kappa^2 + 16\,\kappa + 3}{(\gamma_u + \gamma_v)(2\,\kappa - 2\,\gamma_u + 1)}}}{4} \tag{48}$$

Figure 4 (a) and (b) depict the changes in the optimal frequency and damping ratios in relation to the isolator mass ratio of inerter-based friction bearing for various inerter mass ratios. As the isolator mass ratio rises, the optimal frequency and damping ratios decrease. As the inerter mass ratio rises, the optimal frequency and damping ratios decrease. The displacement response of the isolator's standard deviation has been determined to be

$$\sigma_{w_b}^2 = \frac{-S_0\pi\ (\gamma_v+1)\begin{pmatrix} 2\,\kappa\,\gamma_v\,{\varepsilon_s}^4 + 2\,\gamma_u\,\gamma_v\,{\varepsilon_s}^2{\varepsilon_v}^2 + 2\,{\gamma_v}^2{\varepsilon_s}^2{\varepsilon_v}^2 \\ -\gamma_v\,\kappa\,{\varepsilon_s}^2 - \gamma_u\,\gamma_v\,{\varepsilon_v}^2 - {\gamma_v}^2{\varepsilon_v}^2 - \kappa\,{\varepsilon_s}^2 \\ -{\varepsilon_v}^2\gamma_u - {\varepsilon_s}^2\gamma_v - \gamma_v\,{\varepsilon_v}^2 - {\varepsilon_s}^2 \end{pmatrix}}{2\,\varepsilon_v\,{\varepsilon_s}^2\xi\ (\gamma_u+\gamma_v)\left(\kappa\,{\varepsilon_s}^2 + {\varepsilon_v}^2\gamma_u + \gamma_v\,{\varepsilon_v}^2\right)} \tag{49}$$

The velocity response of the isolator's standard deviation has been determined to be

$$\sigma_{\dot{w}_b}^2 = \frac{\left({\gamma_v}^2 + \gamma_u + \gamma_v\right)\pi\,S_0}{2\varepsilon_v\,\xi\ (\gamma_u+\gamma_v)^2} \tag{50}$$

Further, the optimal design parameters for the inerter-based isolation systems are derived using the H_∞ optimisation method. The harmonic loading is considered as base excitation for this particular purpose.

H_∞ optimisation

The H_∞ optimisation technique is used with the non-dimensional version of Eq. (39) with the initial phase conditions. Furthermore, it has been thought that harmonic base excitation is applied to the isolated structure. Thus, the frequency response function's non-dimensional version is obtained and written as

$$\begin{bmatrix} -\alpha^2+1 & -\alpha^2 \\ -1 & -(\gamma_v+\gamma_u)\,\alpha^2 + 2\,\mathrm{i}\xi\alpha_v\,(\gamma_v+\gamma_u)\,\alpha + \kappa + (\gamma_v+\gamma_u)\,\alpha_v^2 \end{bmatrix} \begin{Bmatrix} W_s \\ W_b \end{Bmatrix} = -\begin{bmatrix} 1 \\ \gamma_v \end{bmatrix} \frac{W_g}{\varepsilon_s^2} \tag{51}$$

The dynamic reaction of the single-degree-of-freedom system is as follows:

$$H_s(\alpha) = \left(\frac{W_s}{W_g}\right)\varepsilon_s^2 = \frac{-\alpha^2\gamma_u + \alpha_v^2\gamma_u + \alpha_v^2\gamma_v + \kappa + \mathrm{i}\left(2\xi\alpha_v\alpha\gamma_u + 2\xi\alpha_v\alpha\gamma_v\right)}{\Phi} \tag{52}$$

The dynamic response of the isolator is calculated as

$$H_b(\alpha) = \left(\frac{W_b}{W_g}\right)\varepsilon_s^2 = \frac{-\alpha^2\gamma_v + \gamma_v + 1}{\Phi} \tag{53}$$

The denominator of Eq. (52) and Eq. (53) is derived as

$$\begin{aligned}\Phi = \; & -\alpha^4\gamma_u - \alpha^4\gamma_v + \alpha^2\alpha_v^2\gamma_u + \alpha^2\alpha_v^2\gamma_v + \alpha^2\kappa + \alpha^2\gamma_u \\ & +\alpha^2\gamma_v - \alpha_v^2\gamma_u - \alpha_v^2\gamma_v + \alpha^2 - \kappa \\ & +\mathrm{i}\left(2\alpha^3\xi\alpha_v\gamma_u + 2\alpha^3\xi\alpha_v\gamma_v - 2\xi\alpha_v\alpha\gamma_u - 2\xi\alpha_v\alpha\gamma_v\right)\end{aligned} \tag{54}$$

The resultant of Eq. (52) is derived to generate constraints for the H_∞ optimization method and represented as follows.

$$|H_s(\alpha)| = \sqrt{\frac{G_1^2 + \xi^2 G_2^2}{G_3^2 + \xi^2 G_4^2}} = \left|\frac{G_2}{G_4}\right|\sqrt{\frac{\frac{G_1^2}{G_2^2} + \xi^2}{\frac{G_3^2}{G_4^2} + \xi^2}} \tag{55}$$

The fixed-point theory is used to generate two constraints from Eq. (55) and express them as

$$\left|\frac{G_1}{G_2}\right|_{\alpha_j} = \left|\frac{G_3}{G_4}\right|_{\alpha_j} \quad \text{and} \quad \left|\frac{G_2}{G_4}\right|_{\alpha_1} = \left|\frac{G_2}{G_4}\right|_{\alpha_2} \tag{56}$$

403 $G_{j=1,2,3,4}$ has been derived as

$$
\begin{aligned}
G_1 &= -\alpha^2\gamma_u + \alpha_v^2\gamma_u + \alpha_v^2\gamma_v + \kappa, \\
G_2 &= 2\alpha\alpha_v\gamma_u + 2\alpha\alpha_v\gamma_v, \\
G_4 &= 2\alpha^3\alpha_v\gamma_u + 2\alpha^3\alpha_v\gamma_v - 2\alpha\alpha_v\gamma_u - 2\alpha\alpha_v\gamma_v, \quad \text{and} \\
G_3 &= \begin{array}{c} -\alpha^4\gamma_u - \alpha^4\gamma_v + \alpha^2\alpha_v^2\gamma_u + \alpha^2\alpha_v^2\gamma_v + \alpha^2 \\ +\alpha^2\kappa + \alpha^2\gamma_u + \alpha^2\gamma_v - \alpha_v^2\gamma_u - \alpha_v^2\gamma_v - \kappa \end{array}
\end{aligned}
\tag{57}
$$

405 The first expression of the Eq. (56) substitutes Eq. (57).

$$
\begin{array}{c}
\left(2\gamma_u^2 + 3\gamma_u\gamma_v + \gamma_v^2\right)\alpha^4 \\
+\left(\begin{array}{c} -2\alpha_v^2\gamma_u^2 - 4\alpha_v^2\gamma_u\gamma_v - 2\alpha_v^2\gamma_v^2 - 2\kappa\gamma_u - 2\kappa\gamma_v \\ -2\gamma_u^2 - 3\gamma_u\gamma_v - \gamma_v^2 - \gamma_u - \gamma_v \end{array}\right)\alpha^2 \quad = 0 \\
+2\alpha_v^2\gamma_u^2 + 4\alpha_v^2\gamma_u\gamma_v + 2\alpha_v^2\gamma_v^2 + 2\kappa\gamma_u + 2\kappa\gamma_v
\end{array}
\tag{58}
$$

407 Equation (58) is written as

$$
\alpha^4 + \left(-\alpha_1^2 - \alpha_2^2\right)\alpha^2 + \alpha_1^2\alpha_2^2 = 0 \tag{59}
$$

409 The summation of the two roots, i.e. $\alpha_1^2 + \alpha_2^2$, are derived after comparing Eq. (58) and Eq. (59).

$$
\alpha_1^2 + \alpha_2^2 = \frac{\left(2\gamma_u + 2\gamma_v\right)\alpha_v^2 + 2\kappa + 2\gamma_u + \gamma_v + 1}{2\gamma_u + \gamma_v} \tag{60}
$$

411 Equation (57) is substituted in the second expression of the Eq. (56).

$$
\alpha_1^2 + \alpha_2^2 = 2 \tag{61}
$$

413 Equation (60) and Eq. (61) are equating to derive the mathematical expression for the optimal
414 natural frequency of the isolator. The real root with the positive value is considered from the

derivation to achieve the optimal natural frequency of the isolator.

$$(\alpha_v)_{\text{opt}} = \frac{\sqrt{2}\sqrt{(\gamma_u+\gamma_v)\,(2\kappa-2\gamma_u-\gamma_v+1)}}{2\gamma_u+2\gamma_v} \tag{62}$$

Equation (55) is squared and partially differentiated with respect to the damping ratio of the isolator to derive its optimal value and the mathematical expression is derived as

$$\left.\frac{\partial|H_s(\alpha)|^2}{\partial\alpha^2}\right|_{\alpha_{1,2}^2} = 0 \quad \text{and} \quad (\xi)_{\text{opt}} = \sqrt{\frac{\xi_1^2+\xi_2^2}{2}} \tag{63}$$

Applying the first expression of Eq. (63), the optimal damping ratio is derived as

$$\begin{aligned} &B_1\xi^4 + B_2\xi^2 + B_3 = 0, \\ &B_1 = -32\alpha_{1,2}^4\alpha_v^4\,(\gamma_u+\gamma_v)^4\left(\alpha_{1,2}^2-1\right), \\ &\xi_{1,2}^2 = \frac{-B_2 \pm \sqrt{B_2^2-4B_1B_3}}{2B_1} \end{aligned} \tag{64}$$

$$
\begin{aligned}
B_2 = &\left(-16\alpha_v^2\gamma_u^4 - 56\alpha_v^2\gamma_u^3\gamma_v - 76\alpha_v^2\gamma_u^2\gamma_v^2 - 48\alpha_v^2\gamma_u\gamma_v^3 - 12\alpha_v^2\gamma_v^4 \right)\alpha_{1,2}^8 \\
&+\begin{pmatrix} 32\alpha_v^4\gamma_u^4 + 112\alpha_v^4\gamma_u^3\gamma_v + 144\alpha_v^4\gamma_u^2\gamma_v^2 + 80\alpha_v^4\gamma_u\gamma_v^3 + 16\alpha_v^4\gamma_v^4 + 32\kappa\,\alpha_v^2\gamma_u^3 \\ +80\kappa\,\alpha_v^2\gamma_u^2\gamma_v + 64\kappa\,\alpha_v^2\gamma_u\gamma_v^2 + 16\kappa\,\alpha_v^2\gamma_v^3 + 16\alpha_v^2\gamma_u^4 + 64\alpha_v^2\gamma_u^3\gamma_v + 16\alpha_v^2\gamma_v^3 \\ +96\alpha_v^2\gamma_u^2\gamma_v^2 + 64\alpha_v^2\gamma_u\gamma_v^3 + 16\alpha_v^2\gamma_v^4 + 16\alpha_v^2\gamma_u^3 + 48\alpha_v^2\gamma_u^2\gamma_v + 48\alpha_v^2\gamma_u\gamma_v^2 \end{pmatrix}\alpha_{1,2}^6 \\
&+\begin{pmatrix} -16\alpha_v^6\gamma_u^4 - 64\alpha_v^6\gamma_u^3\gamma_v - 96\alpha_v^6\gamma_u^2\gamma_v^2 - 64\alpha_v^6\gamma_u\gamma_v^3 - 16\alpha_v^6\gamma_v^4 - 32\kappa\,\alpha_v^4\gamma_u^3 \\ -96\kappa\,\alpha_v^4\gamma_u^2\gamma_v - 96\kappa\,\alpha_v^4\gamma_u\gamma_v^2 - 32\kappa\,\alpha_v^4\gamma_v^3 - 32\alpha_v^4\gamma_u^4 - 112\alpha_v^4\gamma_u^3\gamma_v \\ -144\alpha_v^4\gamma_u^2\gamma_v^2 - 80\alpha_v^4\gamma_u\gamma_v^3 - 16\alpha_v^4\gamma_v^4 - 8\alpha_v^4\gamma_u^3 - 24\alpha_v^4\gamma_u^2\gamma_v - 24\alpha_v^4\gamma_u\gamma_v^2 \\ -8\alpha_v^4\gamma_v^3 - 16\kappa^2\alpha_v^2\gamma_u^2 - 32\kappa^2\alpha_v^2\gamma_u\gamma_v - 16\kappa^2\alpha_v^2\gamma_v^2 - 32\kappa\,\alpha_v^2\gamma_u^3 \\ -80\kappa\,\alpha_v^2\gamma_u^2\gamma_v - 64\kappa\,\alpha_v^2\gamma_u\gamma_v^2 - 16\kappa\,\alpha_v^2\gamma_v^3 - 8\alpha_v^2\gamma_u^3\gamma_v - 20\alpha_v^2\gamma_u^2\gamma_v^2 \\ -16\alpha_v^2\gamma_u\gamma_v^3 - 4\alpha_v^2\gamma_v^4 - 8\kappa\,\alpha_v^2\gamma_u^2 - 16\kappa\,\alpha_v^2\gamma_u\gamma_v - 8\kappa\,\alpha_v^2\gamma_v^2 - 8\alpha_v^2\gamma_u^3 \\ -24\alpha_v^2\gamma_u^2\gamma_v - 24\alpha_v^2\gamma_u\gamma_v^2 - 8\alpha_v^2\gamma_v^3 - 4\alpha_v^2\gamma_u^2 - 8\alpha_v^2\gamma_u\gamma_v - 4\alpha_v^2\gamma_v^2 \end{pmatrix}\alpha_{1,2}^4 \\
&+\begin{pmatrix} 16\alpha_v^6\gamma_u^4 + 64\alpha_v^6\gamma_u^3\gamma_v + 96\alpha_v^6\gamma_u^2\gamma_v^2 + 64\alpha_v^6\gamma_u\gamma_v^3 + 16\alpha_v^6\gamma_v^4 + 32\kappa\,\alpha_v^4\gamma_u^3 \\ +96\kappa\,\alpha_v^4\gamma_u^2\gamma_v + 96\kappa\,\alpha_v^4\gamma_u\gamma_v^2 + 32\kappa\,\alpha_v^4\gamma_v^3 + 16\kappa^2\alpha_v^2\gamma_u^2 + 32\kappa^2\alpha_v^2\gamma_u\gamma_v \\ +16\kappa^2\alpha_v^2\gamma_v^2 \end{pmatrix}\alpha_{1,2}^2
\end{aligned} \tag{65}
$$

$$
\begin{aligned}
B_3 = &-2\left(\gamma_u\alpha_{1,2}^2 + (-\gamma_u - \gamma_v)\,\alpha_v^2 - \kappa\right) \\
&\begin{pmatrix} (\gamma_u + \gamma_v)\,\alpha_{1,2}^4 + \left((-\gamma_u - \gamma_v)\,\alpha_v^2 - \kappa - \gamma_u - \gamma_v - 1\right)\alpha_{1,2}^2 \\ +\,(\gamma_u + \gamma_v)\,\alpha_v^2 + \kappa \end{pmatrix} \\
&\begin{pmatrix} (\gamma_u + \gamma_v)\,\gamma_u\alpha_{1,2}^4 - 2\left((\gamma_u + \gamma_v)\,\alpha_v^2 + \kappa\right)(\gamma_u + \gamma_v)\,\alpha_{1,2}^2 \\ +\left((\gamma_u + \gamma_v)\,\alpha_v^2 + \kappa\right)\left((\gamma_u + \gamma_v)\,\alpha_v^2 + \kappa + \gamma_v + 1\right) \end{pmatrix}
\end{aligned} \tag{66}
$$

where the individual roots of the Eq. (58) are α_1^2 and α_2^2. Before obtaining the precise closed-form equation for each root, that is, α_1^2 and α_2^2, the value of $\alpha_1^2 + \alpha_2^2$ from Eq. (61) has been substituted in Eq. (58). Consequently, the precise closed-form expressions for α_1^2 and α_2^2 are obtained as follows:

$$
\alpha_{1,2}^2 = \frac{2\gamma_u + \gamma_v \pm \sqrt{\begin{matrix} -4\alpha_v^2\gamma_u^2 - 6\alpha_v^2\gamma_u\gamma_v - 2\alpha_v^2\gamma_v^2 - 4\kappa\gamma_u \\ -2\kappa\gamma_v + 4\gamma_u^2 + 4\gamma_u\gamma_v + \gamma_v^2 \end{matrix}}}{2\gamma_u + \gamma_v} \tag{67}
$$

To find the optimal closed-form solutions for Eq. (67), Equation (62) is substituted in Eq. (67).

$$\left(\alpha_{1,2}\right)^2_{\text{opt}} = \frac{2\gamma_u + \gamma_v \pm \sqrt{-8\gamma_u\kappa - 4\gamma_v\kappa + 8\gamma_u^2 + 8\gamma_u\gamma_v + 2\gamma_v^2 - 2\gamma_u - \gamma_v}}{2\gamma_u + \gamma_v} \tag{68}$$

Equation (62) and Eq. (68) are substituted in Eq. (64). Accordingly, the optimal damping ratio of the inerter-based friction bearing has been derived.

The variations of optimal frequency and damping ratios are H_∞ optimised friction bearings are shown in Figure 5 (a) and Figure 5 (b). The optimal frequency ratios are lowered when the isolator mass ratio increases. The frequency ratios decrease with a certain range when the amplifier angle increases. The amplifier angle varies from 5^o to 15^o as after 12^o, the damping ratio crosses 1.0. This amount of damping ratio is not economical for construction purposes. To achieve a cost-effective robust design from the H_∞ optimised isolator, the amplifier angle should be less than equal to 12^o, i.e. $\theta \leq 12^o$. The relationship between the amplifier angle and isolator mass ratio determines the optimal frequency and damping ratios. the line graph is adopted to determine the damping ratio variations with respect to the different values of the isolator mass ratio and stiffness ratio. The effect of the stiffness ratio on the optimal damping ratio of the inerter-based friction bearing is presented in this graph.

DYNAMIC RESPONSE EVALUATION

The optimal dynamic responses of the isolated single-degree-of-freedom systems are determined in frequency and time domain. The frequency domain analysis is performed by considering harmonic excitation and random white-noise excitation. For random white-noise excitation, the Clough-Penzien power spectrum (Lin et al. 1989), which is a modified version of the Kanai-Tajimi spectrum is considered.

Frequency domain results

The optimal dynamic responses of the single-degree-of-freedom systems isolated by the H_2 and H_∞ optimised inertial amplifier friction bearings and inerter-based friction bearings are obtained using the above-derived frequency response functions. First, the fixed points of the frequency

regions of the two optimum novel isolators are derived. Later, the optimal dynamic responses of the single-degree-of-freedom systems isolated by the optimum novel isolators are compared with the optimum conventional base isolator-controlled single-degree-of-freedom system's dynamic responses.

The differences between the optimal dynamic responses of the single-degree-of-freedom system isolated by H_2 optimised inertial amplifier friction bearing have been obtained and shown in Figure 6 (a). The frequency response function of the single-degree-of-freedom system is the function of the frequency ratio and damping ratio of the isolator. The optimal frequency (i.e., Eq. (14)) and damping ratios (i.e., Eq. (16)) are involved to obtain this graph. The isolated single-degree-of-freedom system oscillates in their Eigen frequencies at $\xi = 0$ while the response peaks are shifted from Eigen frequencies at $\xi > 0$. The Eigen frequency points are $\alpha = 0.41$ and $\alpha = 1.23$. The maximum displacement of the single-degree-of-freedom system is optimally minimised at $\alpha = 0.4$ and $\alpha = 1.2$. The response peaks are merged into one and oscillate as a single-degree-of-freedom system when $\xi = \infty$. The frequency point is derived at $\alpha = 1$. Figure 6 (b) illustrates the variations between the optimal structural dynamic responses of the single-degree-of-freedom system isolated by H_2 optimised inerter-based friction bearing and the frequency ratio when the isolators have different damping ratios. To get this number, optimal frequency (i.e., Eq. (47)) and damping ratios (i.e., Eq. (48)) are needed. While the response peaks are moved from Eigen frequencies at $\xi > 0$, the isolated single-degree-of-freedom system oscillates in their Eigen frequencies at $\xi = 0$. The values of $\alpha = 0.4773$ and $\alpha = 1.562$ is the Eigen frequency points. At $\alpha = 0.4712$ and $\alpha = 1.441$, the maximum displacement of the single-degree-of-freedom system is optimally reduced. When $\xi = \infty$, the response peaks combine into a single peak and oscillate as a single-degree-of-freedom system. At $\alpha = 1$, the frequency point is calculated.

The differences between the optimal dynamic responses of the single-degree-of-freedom system isolated by H_∞ optimised inertial amplifier friction bearing have been obtained and shown in Figure 7 (a). The frequency response function of the single-degree-of-freedom system is the function of the frequency ratio and damping ratio of the isolator. The optimal frequency (i.e.,

Eq. (30)) and damping ratios (i.e., Eq. (32)) are involved to obtain this graph. The isolated single-degree-of-freedom system oscillates in their Eigen frequencies at $\xi = 0$ while the response peaks are shifted from Eigen frequencies at $\xi > 0$. The Eigen frequency points are $\alpha = 0.4348$ and $\alpha = 1.234$. The maximum displacement of the single-degree-of-freedom system is optimally minimised at $\alpha = 0.4217$ and $\alpha = 1.185$, i.e. the resonating frequency points. The response peaks are merged into one and oscillate as an single-degree-of-freedom system when $\xi = \infty$. The frequency point is derived at $\alpha = 1$. Figure 7 (b) illustrates the variations between the optimal structural dynamic responses of the single-degree-of-freedom system isolated by H_∞ optimised inerter-based friction bearing and the frequency ratio when the isolators have different damping ratios. To get this number, the optimal frequency (i.e., Eq. (62)) and damping ratios (i.e., Eq. (64)) are needed. While the response peaks are moved from Eigen frequencies at $\xi > 0$, the isolated single-degree-of-freedom system oscillates in their Eigen frequencies at $\xi = 0$. The values of $\alpha = 0.2262$ and $\alpha = 1.473$ are the Eigen frequency points. At $\alpha = 1.550$ and $\alpha = 1.443$, i.e. the resonating frequency points, the maximum displacement of the single-degree-of-freedom system is optimally reduced. When $\xi = \infty$, the response peaks combine into a single peak and oscillate as a single-degree-of-freedom system. At $\alpha = 1$, the frequency point is calculated.

The optimal displacements of the single-degree-of-freedom system isolated by the H_2 and H_∞ optimised inertial amplifier friction bearing and inerter-based friction bearing have been obtained using the above-derived frequency response functions and shown in Figure 8 (a) and Figure 8 (b). The optimal system parameters of all H_2 optimised isolators and single-degree-of-freedom systems are listed in Table 1 and Table 2. The optimal system parameters of all H_∞ optimised isolators are listed in Table 3. According to Figure 8 (a), the maximum displacement of uncontrolled structure is obtained as 25. The maximum displacements of the single-degree-of-freedom system isolated by the conventional base isolator, inertial amplifier friction bearing, and inerter-based friction bearing are derived as 11.08, 2.1, and 1.98. Using these derived data, the dynamic response reduction capacity of each novel bearing is derived with respect to the conventional base isolator, and the

mathematical expression is derived as

$$W_{dr}^{\text{inertial amplifier}}\,(\%) = \left(\frac{(H_s)^{\max}_{\text{conventional base isolator}} - (H_s)^{\max}_{\text{inertial amplifier friction bearing}}}{(H_s)^{\max}_{\text{conventional base isolator}}} \right) \times 100 \qquad (69)$$

$$W_{dr}^{\text{inerter}}\,(\%) = \left(\frac{(H_s)^{\max}_{\text{conventional base isolator}} - (H_s)^{\max}_{\text{inerter- based friction bearing}}}{(H_s)^{\max}_{\text{conventional base isolator}} } \right) \times 100 \qquad (70)$$

where $(H_s)^{\max}_{\text{conventional base isolator}}$: Maximum displacement of single-degree-of-freedom system isolated by conventional base isolator. $(H_s)^{\max}_{\text{inertial amplifier friction bearing}}$: Maximum displacement of single-degree-of-freedom system isolated by inertial amplifier friction bearing. $(H_s)^{\max}_{\text{inerter- based friction bearing}}$: Maximum displacement of single-degree-of-freedom system isolated by inerter-based friction bearing. The maximum displacements are substituted in Eq. (69) and Eq. (70). As a result, the inerter-based friction bearing and inertial amplifier friction bearing are significantly 82.13 % and 81.05 % superior to the conventional base isolators. Now, the vibration reduction capacities of H_∞ optimised novel bearings are derived. According to Figure 8 (b), the maximum displacement of uncontrolled structure is obtained as 25. The maximum displacements of the single-degree-of-freedom system isolated by the conventional base isolator, inertial amplifier friction bearing, and inerter-based friction bearing are derived as 7.78, 1.93, and 1.48. The maximum displacements are substituted in Eq. (69) and Eq. (70). As a result, the inerter-based friction bearing and inertial amplifier friction bearing are significantly 80.98 % and 75.19 % superior to the conventional base isolators.

A white noise base excitation has been taken into consideration when developing the strategy described in this section. Therefore, additional investigations are carried out to prove the reliability of the recommended approach in a larger class of seismic excitation scenarios. The Clough-Penzien power spectrum, a modified version of the widely used Kanai-Tajimi spectrum, may be employed as the ground acceleration for this study in order to accomplish this goal. The one-sided PSD that

is present in the process sets it apart.

$$W_{\ddot{w}_g} = S_0 \frac{\omega_h^4 + 4\zeta_h^2\omega_h^2\omega^2}{\left(\omega_h^2 - \omega^2\right)^2 + 4\zeta_h^2\omega_h^2\omega^2} \frac{\omega^4}{\left(\omega_g^2 - \omega^2\right)^2 + 4\zeta_g^2\omega_g^2\omega^2} \tag{71}$$

where the constant power spectral density for random white noise excitation is defined by S_0. The well-known Kanai-Tajimi model's filter parameters are ω_h and ζ_h, respectively, the natural frequency and damping capacity of the soil layer. A second filter that uses the parameters ω_g and ζ_g provides a limited power output for the ground displacement. As $\omega_g \ll \omega_h$, the second quotient approaches unity very quickly, therefore the second filter only impacts the very low range frequencies. The filter parameter values are obtained from (Kiureghian and Neuenhofer 1992) to investigate sites with soils classed as firm, medium, and soft. In this study, the medium soil is considered. The variations of optimal structural displacement of single-degree-of-freedom system isolated by H_2 and H_∞ optimised inertial amplifier friction bearings, inerter-based friction bearings, and the optimum conventional base isolators versus frequency ratio have been shown in Figure 9 (a) and Figure 9 (b). According to the Figure 9 (a), the maximum displacement of uncontrolled structure is obtained as 4.7535×10^7 dB/Hz. The maximum displacements of the single-degree-of-freedom system isolated by the conventional base isolator, inertial amplifier friction bearing, and inerter-based friction bearing are derived as 3.3095×10^7 dB/Hz, 1.1181×10^6 dB/Hz, and 9.3918×10^5 dB/Hz. The maximum displacements are substituted in Eq. (69) and Eq. (70). As a result, the inerter-based friction bearing and inertial amplifier friction bearing are significantly 97.16 % and 96.62 % superior to the conventional base isolators. According to the Figure 9 (b), the maximum displacement of uncontrolled structure is obtained as 4.7535×10^7 dB/Hz. The maximum displacements of the single-degree-of-freedom system isolated by the conventional base isolator, inertial amplifier friction bearing, and inerter-based friction bearing are derived as 1.3780×10^7 dB/Hz, 9.5974×10^5 dB/Hz, and 5.3142×10^5 dB/Hz. The maximum displacements are substituted in Eq. (69) and Eq. (70). As a result, the inerter-based friction bearing and inertial amplifier friction bearing are significantly 96.14 % and 93.03 % superior to the conventional base

isolators.

Time domain results

The optimal design parameters of the optimum friction bearings are obtained precisely in closed form using the optimization techniques of H_2 and H_∞. Following the application of these optimal design parameters, the optimal dynamic responses of the controlled single-degree-of-freedom systems have already been determined using the frequency domain. Now, a numerical study is also used to validate the proposed approaches. The Newmark-beta method is used to determine the nonlinear time history findings. The near-field earthquake records are considered for this time history analysis. The mass of the main structure, $m = 3000$ tons, is indicated. The structure's time interval is expressed as $T = 0.5$ sec. The time period of the structure, $\varepsilon_s = 2\pi/T$, is used to calculate the natural frequency of the structure. $\zeta = 0.02$ is the expected viscous damping ratio of the single-degree-of-freedom systems. Table 4 has a detailed list of the characteristics related to near-field earthquake recordings with pulses. Figure 10 displays the response spectra of the near field earthquake recordings with pulses, accounting for a 5% damping factor. Compared to far-field earthquakes, the near field without pulses, the near field earthquakes with pulses a greater risk to the structures. Therefore, near-field earthquake recordings that contain pulses with a specific vertical component are used in the numerical analysis to determine each damper's vibration reduction capabilities. Using this data, the dynamic responses of the uncontrolled and isolated single-degree-of-freedom systems are derived. The design parameters of the bearings are listed in Table 1. The optimal dynamic response histories of the single-DOF systems isolated by the optimum inertial amplifier friction bearing, inerter-based friction bearing, and conventional base isolator during Loma Prieta earthquake base excitation varied over time are derived and graphically presented in Figure 11. According to the Figure 11 (a), the maximum dynamic response of the uncontrolled single-degree-of-freedom system is obtained as 0.0047 m. The maximum dynamic responses of the single-degree-of-freedom systems isolated by conventional base isolator, inertial amplifier friction, and inerter-based friction bearing are obtained as 0.0028 m, 0.0020 m, and 0.0020 m. The maximum displacements are substituted in Eq. (69) and Eq. (70). As a result, the dynamic

response reduction capacities of the inerter-based friction bearings and inertial amplifier friction bearings are significantly 28.94 % and 29.43 % superior to the conventional base isolators. Now, the effective natural period of the base-isolated buildings is considered 2 secs, 3 secs, and 4 secs. The graphical representation of the displacement response graphs for longer natural periods are shown in Figure 11 (b), Figure 11 (c), and Figure 11 (d). They are typically rather flexible and this is why they are commonly regarded as vulnerable to pulse-like earthquakes. Thus, structural performance for longer natural periods has been considered here for further performance assessment of each novel isolator. According to the Figure 11 (b), the maximum dynamic response of the uncontrolled single-degree-of-freedom system is obtained as 0.0239 m. The maximum dynamic responses of the single-degree-of-freedom systems isolated by conventional base isolator, inertial amplifier friction, and inerter-based friction bearing are obtained as 0.0114 m, 0.0090 m, and 0.0078 m. As a result, the dynamic response reduction capacities of the inerter-based friction bearings and inertial amplifier friction bearings are significantly 21 % and 32.09 % superior to the conventional base isolators. According to the Figure 11 (c), the maximum dynamic response of the uncontrolled single-degree-of-freedom system is obtained as 0.0243 m. The maximum dynamic responses of the single-degree-of-freedom systems isolated by conventional base isolator, inertial amplifier friction, and inerter-based friction bearing are obtained as 0.0194 m, 0.0098 m, and 0.0121 m. As a result, the dynamic response reduction capacities of the inerter-based friction bearings and inertial amplifier friction bearings are significantly 49.81 % and 37.97 % superior to the conventional base isolators. According to the Figure 11 (d), the maximum dynamic response of the uncontrolled single-degree-of-freedom system is obtained as 0.0351 m. The maximum dynamic responses of the single-degree-of-freedom systems isolated by conventional base isolator, inertial amplifier friction, and inerter-based friction bearing are obtained as 0.0193 m, 0.0105 m, and 0.0117 m. As a result, the dynamic response reduction capacities of the inerter-based friction bearings and inertial amplifier friction bearings are significantly 45.64 % and 39.32 % superior to the conventional base isolators. The dynamic response histories are further evaluated for other considered earthquakes. The maximum dynamic responses are listed in Table 5. According to the Table 5, the dynamic

response reduction capacities of the inerter-based friction bearings and inertial amplifier friction bearings are significantly 36.29 % and 37.73 % superior to the conventional base isolators. The optimal acceleration response histories of the single-degree-of-freedom systems isolated by the optimum conventional base isolator, inertial amplifier friction bearing, and inerter-based friction bearing subjected to Loma Prieta earthquake base excitation have been shown in Figure 12. According to the Figure 12, the maximum acceleration response of the uncontrolled single-degree-of-freedom system is obtained as 0.3974 m/s^2. The maximum acceleration responses of the single-degree-of-freedom systems isolated by conventional base isolator, inertial amplifier friction, and inerter-based friction bearing are obtained as 0.1493 m/s^2, 0.0955 m/s^2, and 0.1426 m/s^2. As a result, the acceleration response reduction capacities of the inerter-based friction bearings and inertial amplifier friction bearings are significantly 36.03 % and 4.51 % superior to the conventional base isolators.

SUMMARY AND CONCLUSIONS

Conventional friction bearings have limitations in managing structural vibration. To overcome these limits and improve their seismic performance, inertial amplifiers, and inerters are added to the core material of traditional friction bearings. As a result, this study introduces two types of enhanced friction bearings: inertial amplifier friction bearings and inerter-based friction bearings. These enhanced friction bearings are positioned at the base of single and multi-story buildings, alongside an adjacent retaining wall. The influence of the building on the retaining wall is examined. The governing equations of motion for isolated structures, including impacts, are determined using Newton's second law. The "signum" function formulates the impact in order to obtain analytically optimal closed-form solutions for the design parameters of these enhanced base isolators. The H_2 and H_∞ optimization methods are used to provide the precise closed-form formula for the optimal design parameters. To use the H_2 optimization approach, the statistical linearisation method is used to linearise each nonlinear element of the governing equations of motion.

- According to parametric research, the optimal frequency and damping ratios drop with

increasing isolator mass ratio, increase with increasing amplifier angle, and decrease with increasing isolator mass ratio.

Developing transfer functions is the initial step in acquiring dynamic reactions from isolated structures. Furthermore, the Newmark-beta method is used to confirm the frequency domain analysis results as well as the dynamic response histories acquired for the isolated single-degree-of freedom systems.

- The results show that the inerter-based friction bearing and inertial amplifier friction bearing have much higher dynamic response reduction capacities (97.16 % and 96.62 %) compared to conventional base isolators.

The novelty of this study lies in the introduction of newly developed friction bearings, such as inertial amplifier friction bearings and inerter-based friction bearings, and the exact closed-form expressions of their optimal design parameters. All results are mathematically developed and accurate, making them suitable for practical applications. In addition, theoretically, any answer is valid and may be applied to other problems in the future, such as vibration control of multiple degrees of freedom systems (i.e., conceptualised model of high-rise buildings) and vibration control of nonlinear dynamic systems.

ORCID ID

Sudip Chowdhury: https://orcid.org/0000-0001-6218-4843
Arnab Banerjee: https://orcid.org/0000-0002-3157-6200
Sondipon Adhikari: https://orcid.org/0000-0003-4181-3457

Declaration of competing interest

The authors declare that they have no known competing financial interests or personal relationships that could have appeared to influence the work reported in this paper

Acknowledgement

The authors would like to acknowledge the Inspire faculty grant, grant number DST/ INSPIRE/04/2018/000052, for partial financial support for the project. Sudip Chowdhury would like to acknowledge the MHRD grant and IRD Early-Doc Fellowship received from IIT Delhi during the period of this research work. Sudip Chowdhury would like to acknowledge the Postdoctoral research grant received from The University of Glasgow for the partial financial support for this research work.

Data Availability Statement

All data, models, and code generated or used during the study appear in the submitted article.

REFERENCES

Adhikari, S. and Banerjee, A. (2022). "Enhanced low-frequency vibration energy harvesting with inertial amplifiers." *Journal of Intelligent Material Systems and Structures*, 33(6), 822–838.

Anagnostopoulos, S. A. (2004). "Equivalent viscous damping for modeling inelastic impacts in earthquake pounding problems." *Earthquake Engineering & Structural Dynamics*, 33(8), 897–902.

Balachandran, B. (2003). "Dynamics of an elastic structure excited by harmonic and aharmonic impactor motions." *Journal of Vibration and Control*, 9(3-4), 265–279.

Banerjee, A., Adhikari, S., and Hussein, M. I. (2021). "Inertial amplification band-gap generation by coupling a levered mass with a locally resonant mass." *International Journal of Mechanical Sciences*, 207, 106630.

Cardone, D., Gesualdi, G., and Brancato, P. (2015). "Restoring capability of friction pendulum seismic isolation systems." *Bulletin of Earthquake Engineering*, 13, 2449–2480.

Chowdhury, S. and Banerjee, A. (2023a). "The non-dimensional response spectra of impact oscillators subjected to pulse-type base excitation." *International Journal of Dynamics and Control*, 1–22.

Chowdhury, S. and Banerjee, A. (2023b). "The nonlinear dynamic analysis of optimum nonlinear inertial amplifier base isolators for vibration isolation." *Nonlinear Dynamics*, 1–38.

Chowdhury, S. and Banerjee, A. (2024). "The impacting vibration absorbers." *Applied Mathematical Modelling*, 127, 454–505.

Chowdhury, S., Banerjee, A., and Adhikari, S. (2022). "Optimal negative stiffness inertial-amplifier-base-isolators: Exact closed-form expressions." *International Journal of Mechanical Sciences*, 218, 107044.

Chowdhury, S., Banerjee, A., and Adhikari, S. (2023a). "Nonlinear inertial amplifier resilient friction base isolators for multiple degrees of freedom systems." *Mechanics of Advanced Materials and Structures*, 1–8.

Chowdhury, S., Banerjee, A., and Adhikari, S. (2023b). "The optimal design of negative stiffness inerter passive dampers for structures." *International Journal of Mechanical Sciences*, 108551.

Chowdhury, S., Banerjee, A., and Adhikari, S. (2023c). "The optimum inerter-based additional viscoelastic mass dampers for dynamic response mitigation of structures." *Mechanics Based Design of Structures and Machines*, 1–24.

Chowdhury, S., Banerjee, A., and Adhikari, S. (2024). "Enhancing seismic resilience of nonlinear structures through optimally designed additional mass dampers." *International Journal of Non-Linear Mechanics*, 162, 104717.

Constantinou, M., Mokha, A., and Reinhorn, A. (1990). "Teflon bearings in base isolation ii: Modeling." *Journal of structural engineering*, 116(2), 455–474.

Davies, M. and Balachandran, B. (2000). "Impact dynamics in milling of thin-walled structures." *Nonlinear Dynamics*, 22, 375–392.

De Angelis, M., Giaralis, A., Petrini, F., and Pietrosanti, D. (2019). "Optimal tuning and assessment of inertial dampers with grounded inerter for vibration control of seismically excited base-isolated systems." *Engineering Structures*, 196, 109250.

De Domenico, D. and Ricciardi, G. (2018). "An enhanced base isolation system equipped with optimal tuned mass damper inerter (tmdi)." *Earthquake engineering & structural dynamics*,

47(5), 1169–1192.

Jangid, R. (2021). “Optimum tuned inerter damper for base-isolated structures.” *Journal of Vibration Engineering & Technologies*, 9(7), 1483–1497.

Kelly, J. M. (1986). “Aseismic base isolation: review and bibliography.” *Soil Dynamics and earthquake engineering*, 5(4), 202–216.

Kelly, J. M. and Beucke, K. E. (1983). “A friction damped base isolation system with fail-safe characteristics.” *Earthquake Engineering & Structural Dynamics*, 11(1), 33–56.

Kiureghian, A. D. and Neuenhofer, A. (1992). “Response spectrum method for multi-support seismic excitations.” *Earthquake engineering & structural dynamics*, 21(8), 713–740.

Li, J., Zhao, H., Zhu, S., and Yang, X. (2023). “h_∞ and h_2 optimization of the grounded-type dva attached to damped primary system based on generalized fixed-point theory coupled optimization algorithm.” *Journal of Vibration Engineering & Technologies*, 1–17.

Lin, B., Tadjbakhsh, I., Papageorgiou, A., and Ahmadi, G. (1989). “Response of base-isolated buildings to random excitations described by the clough-penzien spectral model.” *Earthquake engineering & structural dynamics*, 18(1), 49–62.

Liu, F., Wang, J., Zhou, B., Wu, M., He, J., and Bin, J. (2023). “Shaking table study on rubber-sand mixture cored composite block as low-cost isolation bearing for rural houses.” *Journal of Building Engineering*, 76, 107413.

Luo, H., Zhu, H., and Ikago, K. (2023). “Optimal design of negative-stiffness dampers for improved efficiency of structural seismic isolation.” *Journal of Building Engineering*, 68, 106172.

Mostaghel, N. and Khodaverdian, M. (1987). “Dynamics of resilient-friction base isolator (r-fbi).” *Earthquake engineering & structural dynamics*, 15(3), 379–390.

Ou, J., Wu, P., and Guan, X. (2021). “Resilient isolation-structure systems with super-large displacement friction pendulum bearings.” *International Journal of Sustainable Materials and Structural Systems*, 5(1-2), 11–34.

Papageorgiou, C., Houghton, N. E., and Smith, M. C. (2009). “Experimental testing and analysis of inerter devices.

740 Pietrosanti, D., De Angelis, M., and Giaralis, A. (2021). "Experimental seismic performance
741 assessment and numerical modelling of nonlinear inerter vibration absorber (iva)-equipped base
742 isolated structures tested on shaking table." *Earthquake Engineering & Structural Dynamics*,
743 50(10), 2732–2753.
744 Polycarpou, P. C. and Komodromos, P. (2010). "Earthquake-induced poundings of a seismically
745 isolated building with adjacent structures." *Engineering Structures*, 32(7), 1937–1951.
746 Rahgozar, A., Estekanchi, H. E., and Mirfarhadi, S. A. (2023). "On optimal triple friction pendulum
747 base-isolation design for steel moment-frame buildings employing value-based seismic design
748 methodology." *Journal of Building Engineering*, 63, 105494.
749 Roberts, J. B. and Spanos, P. D. (2003). *Random vibration and statistical linearization*. Courier
750 Corporation.
751 Sharma, A. and Jangid, R. (2010). "Seismic response of base-isolated benchmark building with
752 variable sliding isolators." *Journal of Earthquake Engineering*, 14(7), 1063–1091.
753 Shrimali, M. and Jangid, R. (2002). "Seismic response of liquid storage tanks isolated by sliding
754 bearings." *Engineering structures*, 24(7), 909–921.
755 Smith, M. C. (2002). "Synthesis of mechanical networks: the inerter." *IEEE Transactions on*
756 *automatic control*, 47(10), 1648–1662.
757 Smith, M. C. (2020). "The inerter: a retrospective." *Annual Review of Control, Robotics, and*
758 *Autonomous Systems*, 3, 361–391.
759 Smith, M. C. and Wang, F.-C. (2004). "Performance benefits in passive vehicle suspensions em-
760 ploying inerters." *Vehicle system dynamics*, 42(4), 235–257.
761 Sun, H., Zuo, L., Wang, X., Peng, J., and Wang, W. (2019). "Exact h2 optimal solutions to inerter-
762 based isolation systems for building structures." *Structural Control and Health Monitoring*,
763 26(6), e2357.
764 Swift, S., Smith, M. C., Glover, A., Papageorgiou, C., Gartner, B., and Houghton, N. E. (2013).
765 "Design and modelling of a fluid inerter." *International Journal of Control*, 86(11), 2035–2051.
766 Taniguchi, T., Der Kiureghian, A., and Melkumyan, M. (2008). "Effect of tuned mass damper on

displacement demand of base-isolated structures." *Engineering Structures*, 30(12), 3478–3488.

Yilmaz, C., Hulbert, G. M., and Kikuchi, N. (2007). "Phononic band gaps induced by inertial amplification in periodic media." *Physical Review B*, 76(5), 054309.

Zhao, Z., Zhang, R., Wierschem, N. E., Jiang, Y., and Pan, C. (2021). "Displacement mitigation–oriented design and mechanism for inerter-based isolation system." *Journal of Vibration and Control*, 27(17-18), 1991–2003.

List of Tables

TABLE 1. The optimal system parameters for H_2 optimised isolators.

System	**Proposed by**	H_2 **optimization**	
		α_v	ξ
Inertial amplifier friction bearing	This study	0.4829	0.4302
Inerter-based friction bearing	This study	0.7071	0.6383
Conventional base isolator	Kelly and Beucke (Kelly and Beucke 1983)	0.64	0.056

Conventional base isolator: base mass ratio (μ_B) = 0.9; inertial amplifier friction bearing: isolator mass ratio (μ_{iv}) = 0.70, amplifier mass ratio (μ_r = 0.1), and inertial angle = 10^o; inerter-based friction bearing: isolator mass ratio (μ_v) = 0.80, inerter mass ratio (μ_u) = 0.10, Mass ratio: $\mu_B = \mu_{iv} + 2\mu_r = \mu_v + \mu_u = 0.9$.

TABLE 2. The system parameters of single-degree-of-freedom system (uncontrolled and controlled single-degree-of-freedom systems).

Name	Symbol	Values
Damping ratio	ζ	0.02

TABLE 3. The optimal system parameters for H_∞ optimised isolators.

System	**Proposed by**	H_∞ **optimization**	
		α_v	ξ
Inertial amplifier friction bearing	This study	0.516496	0.512315
Inerter-based friction bearing	This study	0.235702	0.962788
Conventional base isolator	Constantinou et al. (Constantinou et al. 1990)	0.25	0.05

Conventional base isolator: base mass ratio (μ_B) = 0.9; inertial amplifier friction bearing: isolator mass ratio (μ_{iv}) = 0.70, amplifier mass ratio (μ_r = 0.1), and inertial angle = 10^o; inerter-based friction bearing: isolator mass ratio (μ_v) = 0.80, inerter mass ratio (μ_u) = 0.10, Mass ratio: $\mu_B = \mu_{iv} + 2\mu_r = \mu_v + \mu_u = 0.9$.

TABLE 4. The details of near-field seismic records with pulses (https://peer.berkeley.edu/peer-strong-ground-motion-databases).

Earthquake	Year	M_w	Recording station	Vs_{30}(m/s)	Component	E_s (km)	PGA,g
Irpinia, Italy-01	1980	6.9	Sturno	1000	MUL009	30.4	0.31
Superstition Hills-02	1987	6.5	Parachute Test Site	349	SUPERST	16.0	0.42
Loma Prieta	1989	6.9	LOMAP	371	HEC000	27.2	0.38
Erzican, Turkey	1992	6.7	Erzincan 11	275	ERZIKAN	9.0	0.49
Cape Mendocino	1992	7.0	CAPEMEND	713	NIS090	4.5	0.63
Landers	1992	7.3	Lucerne	685	LANDERS	44.0	0.79
Northridge-01	1994	6.7	Rinaldi Receiving Sta	282	NORTHR	10.9	0.87
Kocaeli, Turkey	1999	7.5	Izmit	811	KOCAELI	5.3	0.22
Chi-Chi, Taiwan	1999	7.6	TCU065	306	CHICHI	26.7	0.82
Chi-Chi, Taiwan	1999	7.6	TCU102	714	CHICHI	45.6	0.29
Duzce, Turkey	1999	7.1	Duzce	276	DUZCE	1.6	0.52

TABLE 5. The study investigates the maximum dynamic responses of uncontrolled and isolated single-degrees-of-freedom systems subjected to near-field earthquake recordings with pulses. The maximum dynamic responses are substituted in Eq. (69) and Eq. (70) to obtain the optimal dynamic response reduction capacity of inertial amplifier friction bearing and inerter-based friction bearing with respect to the conventional base isolator.

Earthquake	H_s^{max} **(m)**				W_{dr} (%)	
	Uncontrolled	**Conventional base isolator**	**Inertial amplifier friction bearing**	**Inerter-based friction bearing**	**Inertial amplifier friction bearing**	**Inerter-based friction bearing**
Irpinia, Italy-01	0.0055	0.0038	0.0021	0.0022	43.87	42.53
Superstition Hills-02	0.0067	0.0057	0.0038	0.0034	33.52	40.70
Loma Prieta	0.0047	0.0028	0.0020	0.0020	28.94	29.43
Erzican, Turkey	0.0063	0.0031	0.0021	0.0023	31.71	25.37
Cape Mendocino	0.0094	0.0088	0.0045	0.0047	49.60	46.72
Landers	0.0045	0.0034	0.0024	0.0024	30.54	28.95
Northridge-01	0.0063	0.0034	0.0027	0.0026	19.66	25.30
Kocaeli, Turkey	0.0031	0.0022	0.0012	0.0012	47.72	46.21
Chi-Chi, Taiwan	0.0088	0.0071	0.0039	0.0038	45.20	46.44
Chi-Chi, Taiwan	0.0052	0.0035	0.0027	0.0025	22.55	26.90
Duzce, Turkey	0.0081	0.0065	0.0035	0.0028	45.95	56.48
Average	0.006236	0.004573	0.002809	0.002718	36.29636	37.73

List of Figures

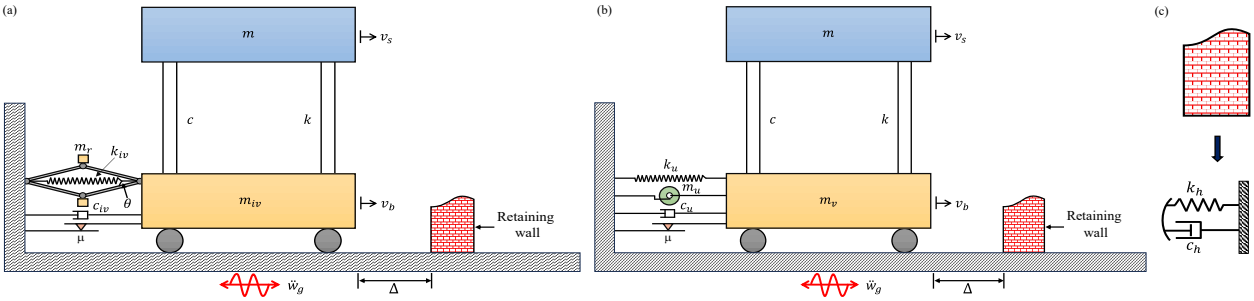

Fig. 1. Two single-degree-of-freedom systems with an adjacent structure (retaining wall) are isolated by (a) inertial amplifier friction bearing and (b) inerter-based friction bearing subjected to base excitation. (c) The schematic diagram of the retaining wall.

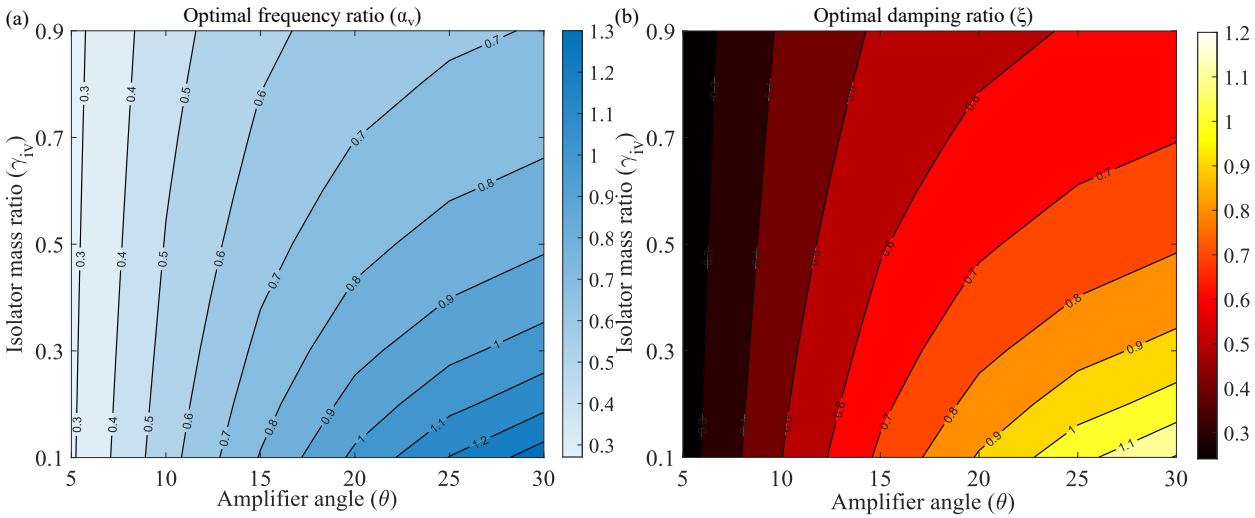

Fig. 2. The contour plots of optimal (a) frequency ratio (α_v) and (b) damping ratio (ξ) of the isolator for different values of isolator mass ratio (γ_{iv}) $\in [0.1, 0.9]$ and amplifier angle (θ) $\in [5^o, 30^o]$. The optimal frequency and damping ratios are the function of the isolator mass ratio and amplifier angle.

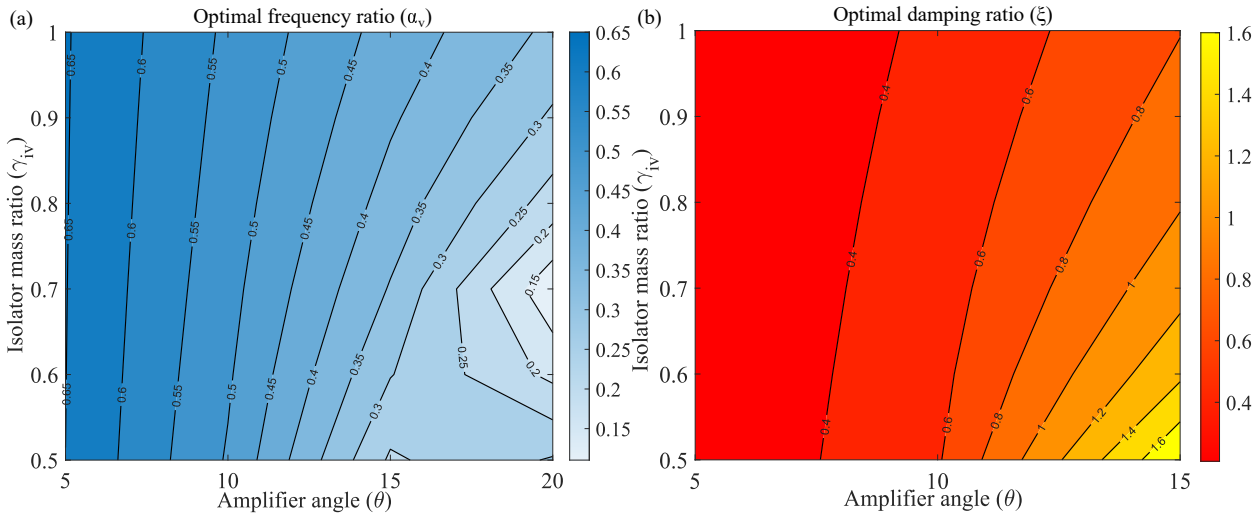

Fig. 3. For various values of the amplifier angle $(\theta) \in [5^o, 20^o]$ and the isolator mass ratio $(\gamma_{iv}) \in [0.5, 1]$, the contour plots of the optimal (a) frequency ratio (α_v) and (b) damping ratio (ξ) of the isolator are presented. Specifically, the amplifier angle varies from 5^o to 15^o as after 12^o, the damping ratio crosses 1.0. This amount of damping ratio is not economical for construction purposes. To achieve a cost-effective robust design from the H_∞ optimised isolator, the amplifier angle should be less than equal to 12^o, i.e. $\theta \leq 12^o$. The relationship between the amplifier angle and isolator mass ratio determines the optimal frequency and damping ratios.

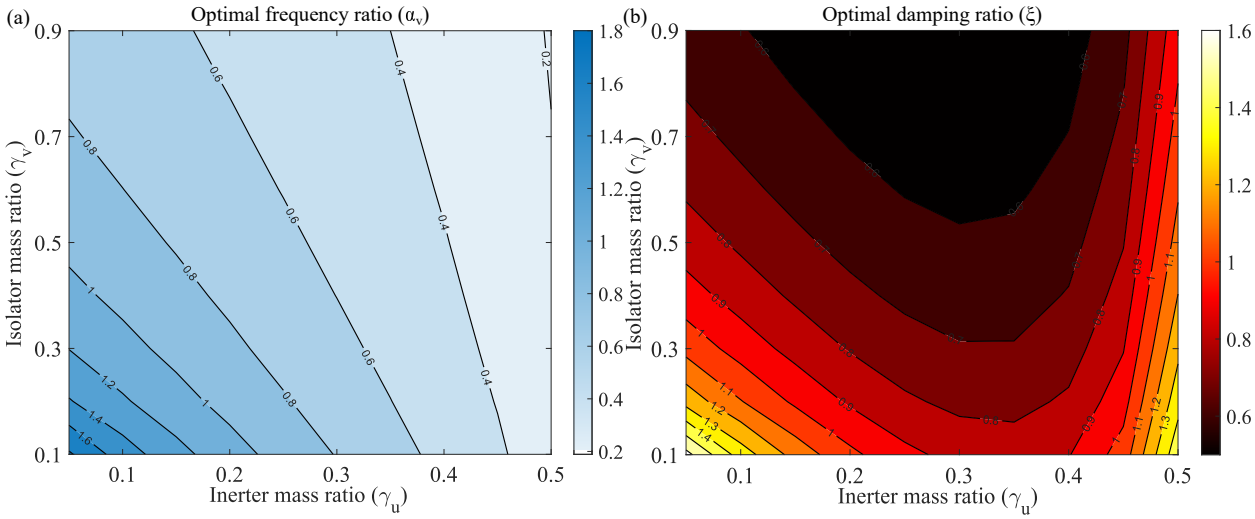

Fig. 4. The variations of the optimal (a) frequency ratio (α_v) and (b) damping ratio (ξ) of the isolator for different values of isolator mass ratio (γ_v) $\in [0.1, 0.9]$ and inerter mass ratio (γ_u) $\in [0.1, 0.5]$ are shown in this contour graph. The optimal frequency and damping ratios are the function of the isolator mass ratio and inerter mass ratio.

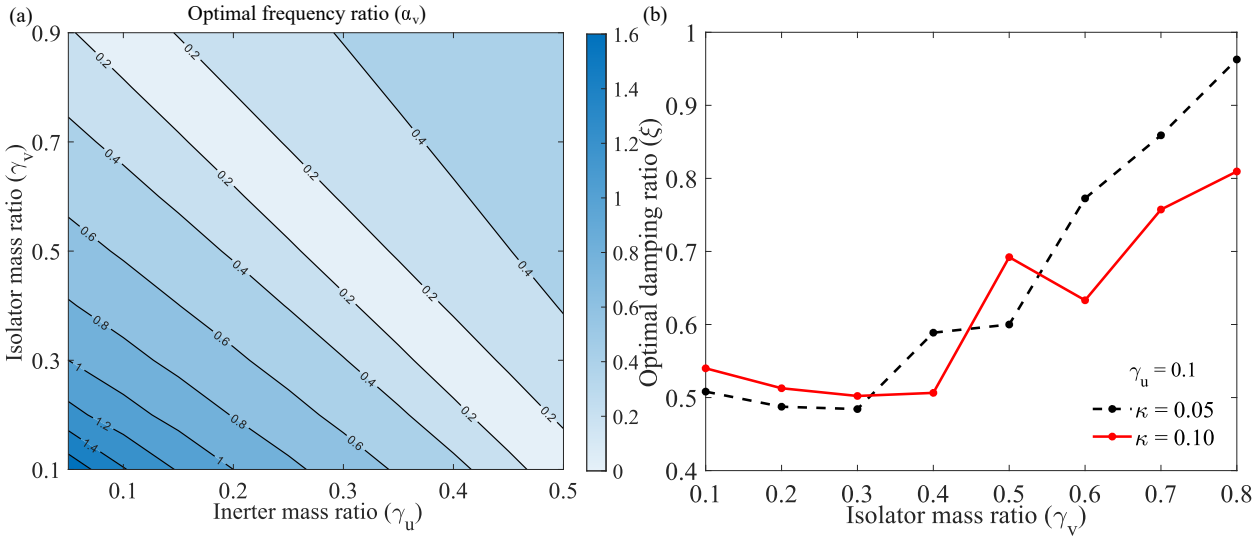

Fig. 5. (a) For various values of the inerter mass ratio $(\gamma_u) \in [0.1, 0.5]$ and the isolator mass ratio $(\gamma_v) \in [0.1, 0.9]$, the contour plots of the optimal frequency ratio (α_v) of the inerter-based friction bearing are presented. The nature of the contour graphs are same. Therefore, (b) the line graph is adopted to determine the damping ratio variations with respect to the different values of isolator mass ratio and stiffness ratio. The effect of stiffness ratio on the optimal damping ratio of the inerter-based friction bearing is presented in this graph.

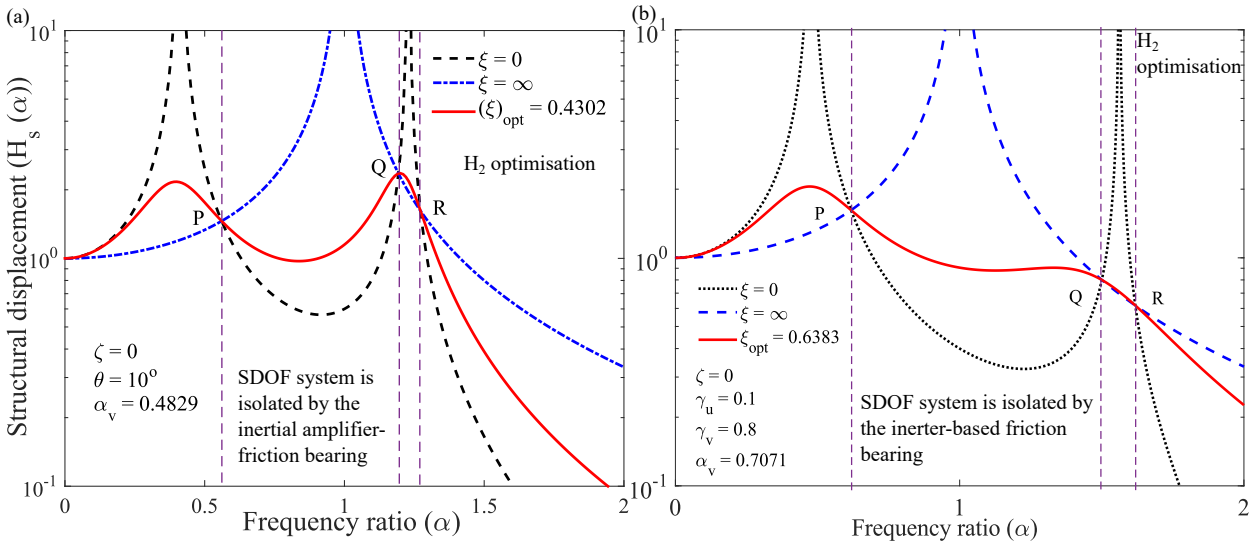

Fig. 6. The variations of optimal structural displacement of single-degree-of-freedom system isolated by the H_2 optimised (a) inertial amplifier friction bearing and (b) inerter-based friction bearing versus frequency ratio with the presence of different damping ratios of isolators. The damping ratio of the single-degree-of-freedom system is considered zero, i.e. $\zeta = 0$.

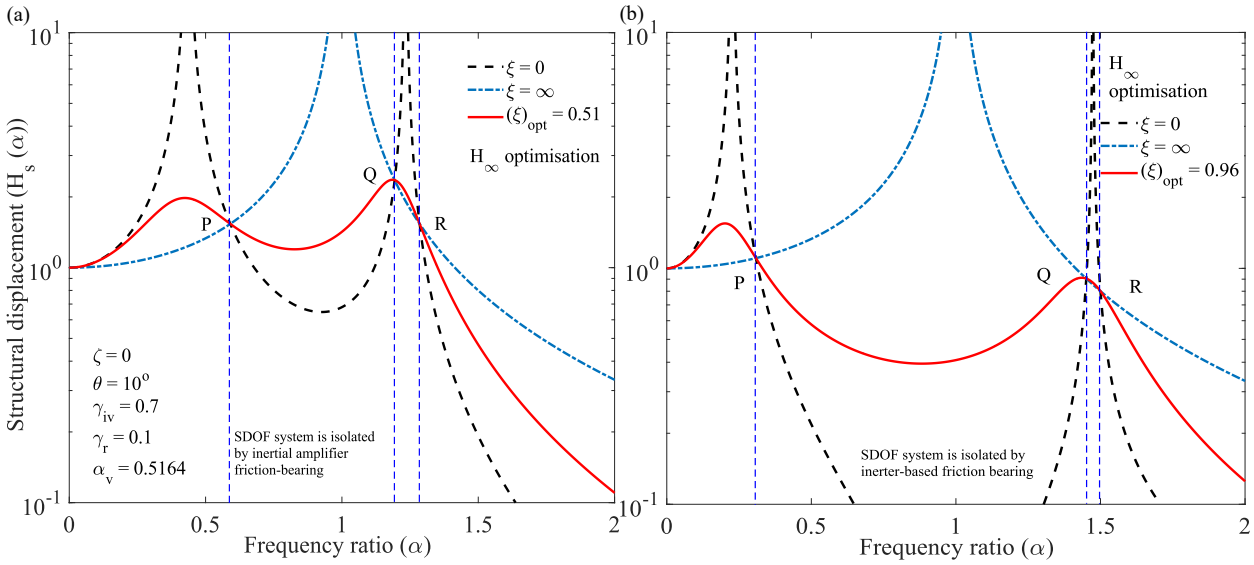

Fig. 7. The variations of optimal structural displacement of single-degree-of-freedom system isolated by the H_∞ optimised (a) inertial amplifier friction bearing and (b) inerter-based friction bearing versus frequency ratio with the presence of different damping ratios of isolators. The damping ratio of the single-degree-of-freedom system is considered zero, i.e. $\zeta = 0$.

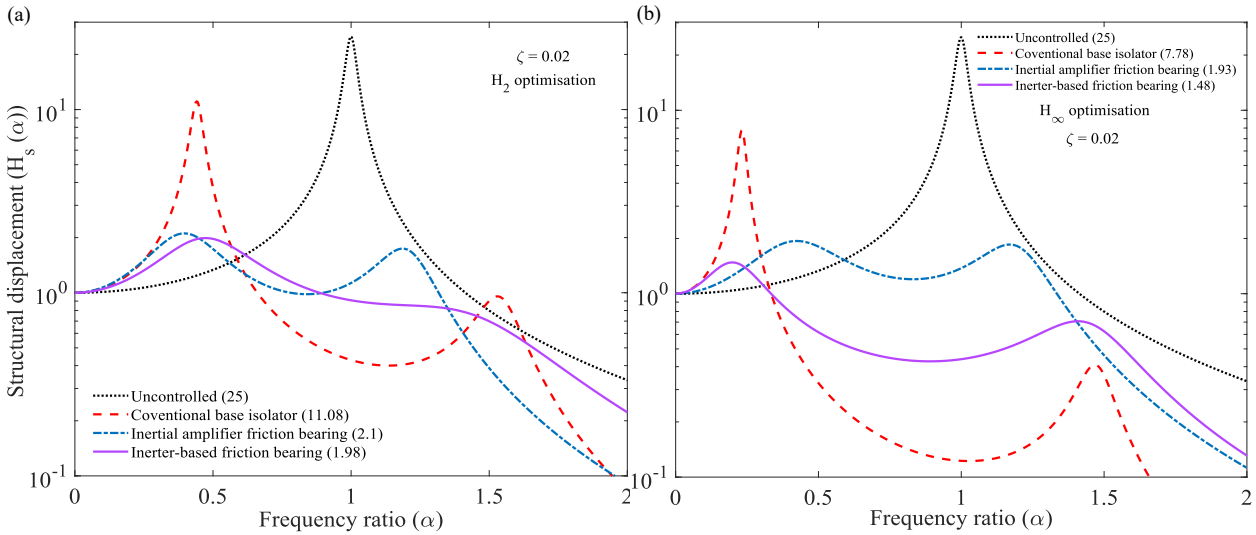

Fig. 8. The variations of optimal structural displacement of single-degree-of-freedom system isolated by (a) H_2 and (b) H_∞ optimised inertial amplifier friction bearing and inerter-based friction bearing versus frequency ratio. The damping ratio of the single-degree-of-freedom system is considered zero, i.e. $\zeta = 0.02$.

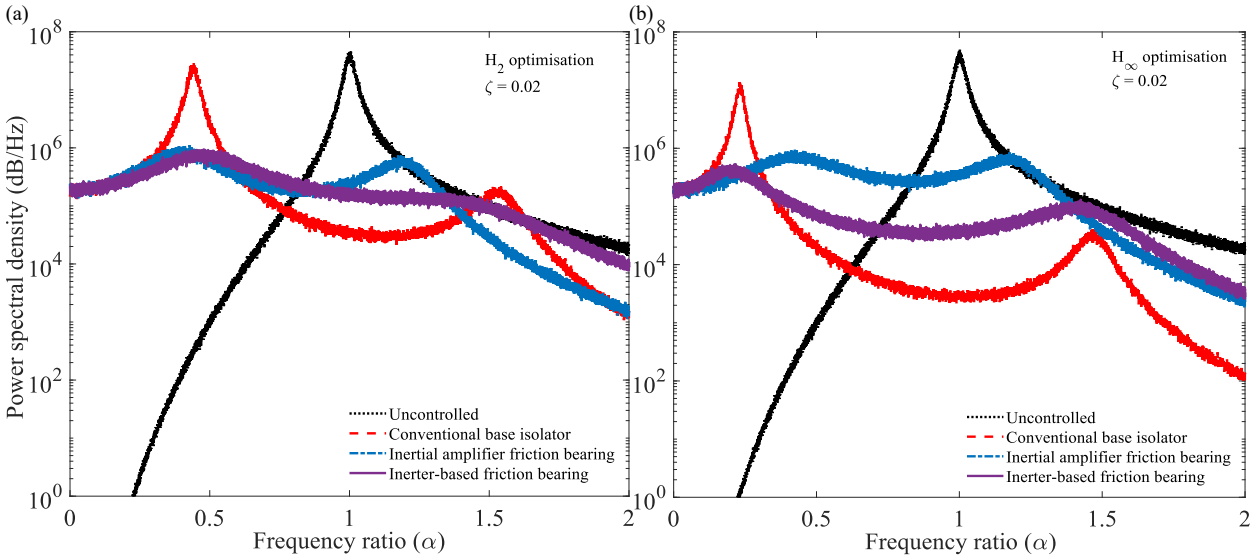

Fig. 9. Differences in the optimal structural displacement of a system with a single-degree-of-freedom isolated by (a) H_2 and (b) H_∞ optimised inertial amplifier friction bearing and inerter-based friction bearing concerning frequency ratio. The optimum conventional base isolators are considered for this study. The optimal design parameters for all optimum isolators are listed in Table 1 and Table 3. The damping ratio of the single-degree-of-freedom system is considered zero, i.e. $\zeta = 0.02$.

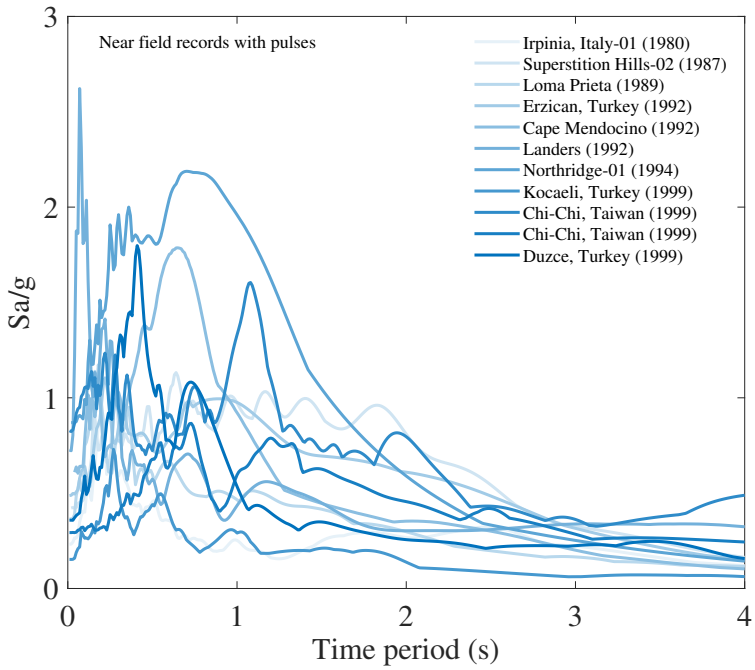

Fig. 10. The response spectra of the near field earthquake recordings with pulses, using a damping factor of 5%.

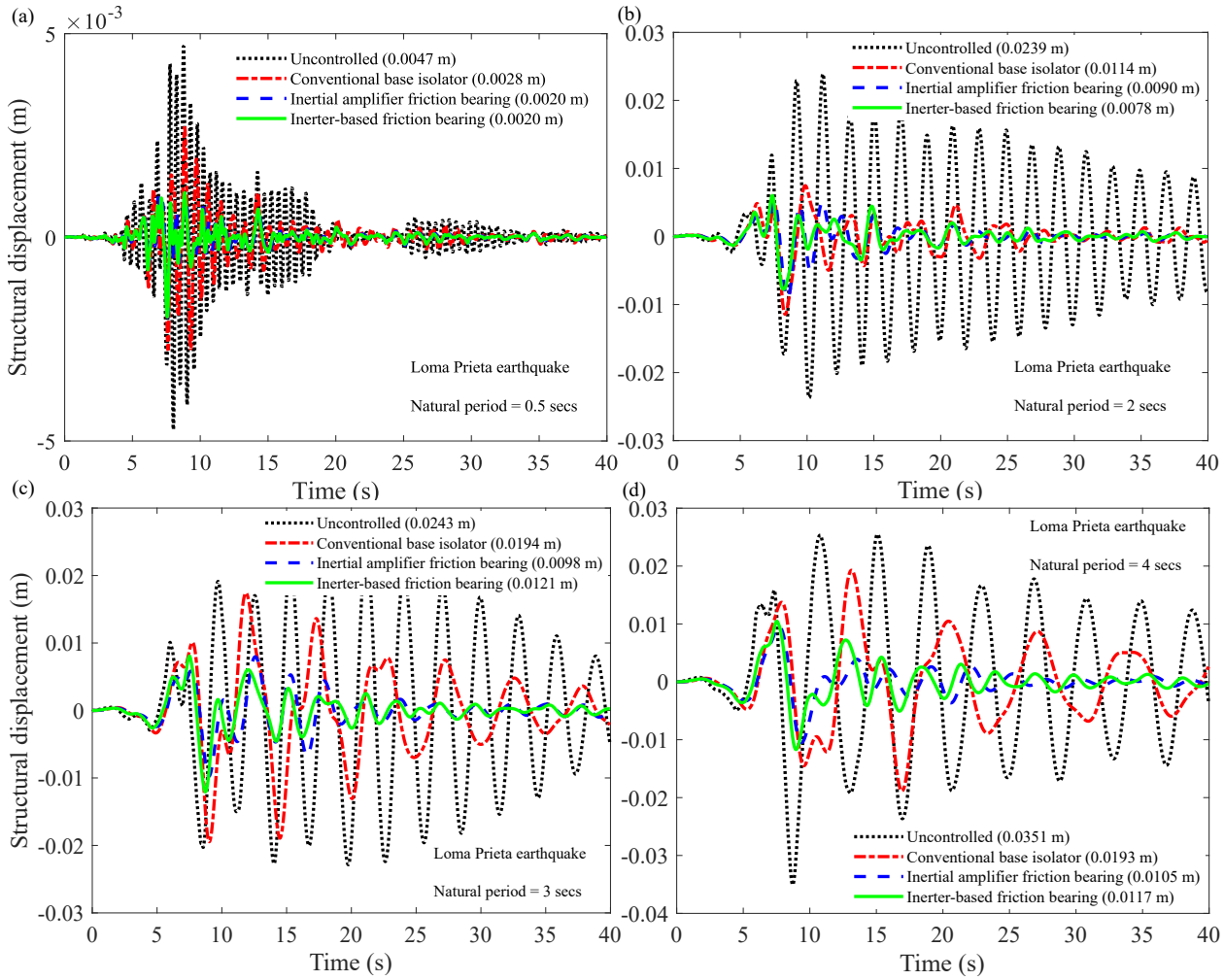

Fig. 11. The optimal dynamic response histories of the single-degree-of-freedom systems isolated by the optimum conventional base isolator, inertial amplifier friction bearing, and inerter-based friction bearing subjected to Loma Prieta earthquake base excitation for the natural period of (a) 0.5 secs, (b) 2 secs, (c) 3 secs, and (d) 4 secs.

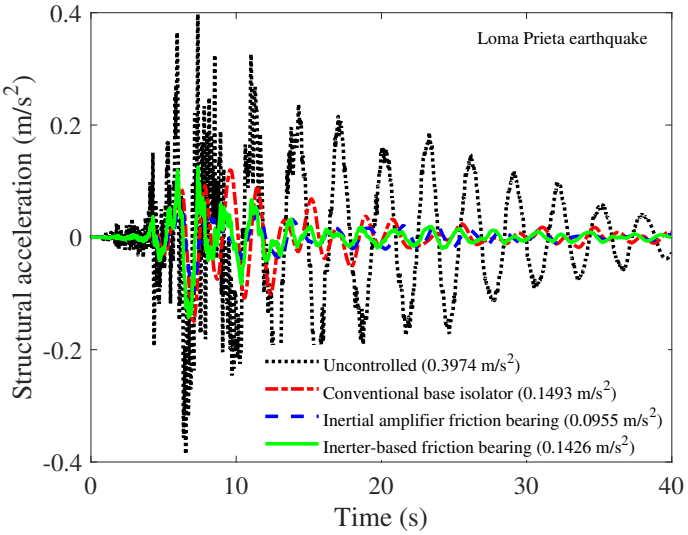

Fig. 12. The optimal acceleration response histories of the single-degree-of-freedom systems isolated by the optimum conventional base isolator, inertial amplifier friction bearing, and inerter-based friction bearing subjected to Loma Prieta earthquake base excitation.